SmartWood: field-based analysis of large wood movement dynamics using inertial measurement units (IMUs)

Gabriel Spreitzer[1*], Isabella Schalko[2], Robert M. Boes[1] and Volker Weitbrecht[1]

Abstract

Wood plays an important ecological role in rivers. Yet challenges arise when large wood (LW) is mobilised and transported during floods. Due to a lack of quantitative data, movement behaviour of LW during floods is still not well understood to date. A proof-of-concept study was conducted at three Swiss rivers to test state-of-the-art sensor-tagged logs, so-called "SmartWood" and collect quantitative field-scale data about LW movement behaviour. The experiments utilised innovative inertial measurement units (IMUs), which have been developed at the Laboratory of Hydraulics, Hydrology and Glaciology (VAW) at ETH Zurich and implanted into wood logs (SmartWood) at prototype scale. Each IMU comprised three individual sensors (gyroscope, accelerometer, and magnetometer) and was equipped with an on-board processor, an AA battery (4.35 V), a memory (8 MB), and a Wi-Fi transmitter (100 m) for data transfer. After successful initial verification tests of the sensors, the IMUs were installed into debranched wood logs, measuring 4.35 m in length and 0.33 m in diameter. At the time of the field experiments, each Smart-Wood-log weighted between 170 and 220 kg, yielding a density of roughly 500 kg·m^{-3}. At the Limmat, Thur, and Grosse Melchaa Rivers in Switzerland, innovative yet discontinuous data were obtained. Results revealed consistent movement dynamics across all field sites. Specifically, we observed positive yaw movement during transport of SmartWood along the left river bank and negative yaw movement along the right river bank. Furthermore, interactions of SmartWood with channel boundaries, riparian vegetation, and objects (e.g., ferry dock) were registered and quantified, even when the SmartWood-log was transported out of sight of traditional sensing methods. The conducted field experiments enabled the initial testing of SmartWood in the field and exposed critical limitations of the IMUs and software algorithms for the reconstruction and analysis of floating LW dynamics. The gained knowledge and introduced sensing method will benefit the quantitative assessment of LW dynamics in rivers to maintain safety and functionality for instream structures (e.g., considering LW movement dynamics for the robust design of LW retention and guiding structures), but also river restoration projects and numerical models that rely on quantitative field-scale data.

Highlights

- Field experiments grant novel insights into large wood (LW) dynamics during floods.
- Applying inertial measurement units (IMUs) in flood-borne wood logs—SmartWood.
- Obtaining quantitative data of LW movement dynamics.

*Correspondence:
Gabriel Spreitzer
gspr390@aucklanduni.ac.nz
Full list of author information is available at the end of the article

- Reconstruction of LW movement and log orientation during floods.
- Lower flow depths and more turbulent flow conditions magnify stress on LW.

Introduction

Large wood (LW) in fluvial environments

Wood is an essential element in rivers, regulating stream power and sediment budgets while enhancing habitat diversity [2, 77]. However, changing climatic conditions, unregulated land-use strategies and reduced dead-wood management are noticeably boosting the production of large quantities of wood in catchments [92], outbalancing the benefits of wood in rivers while increasing the danger potential during floods. The recruitment of wood by the river after natural disasters such as fires, droughts, wind and snow-break, or commercial forestry is often happening within a short period of time after the respective natural disaster [67]. As soon as wood enters the riparian zone, it is commonly referred to as large wood (LW), if its dimensions exceed 1 m in length and 0.1 m in diameter [59, 99]. In the course of heavy precipitation, LW may be quickly mobilised and transported by the flow, yet underlying movement dynamics are barely documented due to a lack of applicable sensing techniques. During floods, LW poses a hazard for impacts at instream structures [36, 85] but also bridge scour and backwater effects in case of LW accumulations [33, 57, 76, 89]. Incidents involving wood in transit and damage due to LW accumulations at critical instream infrastructure are increasingly reported all over the world, and thus require more attention and an improved understanding of intrinsic movement dynamics of LW during floods [20, 29, 44, 91].

Brief history of LW tracking

The desire to investigate and better understand LW movement dynamics has a long history and may have started with the advent of extensive logging practices during the early timber industries in the sixteenth century [14, 27], at a time where natural but also artificially generated floods represented the main transportation mechanism for logs. One of the first scientific observations of LW transport and their effects on stream channels was reported by Cormack [25]. Over the following decades researchers investigated the importance of LW for stream health and biodiversity [18, 56, 97] while the study of wood dynamics in rivers also gained popularity [93], fostering the development of methodologies to map and track LW in fluvial environments [2, 37, 59]. In the meantime, experimenting with LW under controlled conditions in the laboratory but also the employment of digital sensing techniques (e.g., cameras) has become state-of-the-art for the tracking and measuring of wood transport in fluvial systems [17, 43, 47]. However, complex wood movement processes still remain unexplored, due to a lack of quantitative data [15]. Besides flume and field-scale experiments with LW, public camera footage of wood movement during floods was shown to provide valuable documentation for scientific evaluation of LW transport behaviour [70]. An alternative method proposed by Comiti et al. [23] used metal-tags to investigate the mobilisation and transport of LW throughout a stream reach. The tagging-method was later used by Warren and Kraft [98] and eventually developed into studies using passive and active remote frequency identification tags (RFID) and GPS [49, 68, 78]. Findings confirm that LW dimensions with respect to stream width and flow depth strongly correlate to its mobility [9, 37, 59, 98]. Accordingly, smaller LW pieces were transported the furthest within the same period of time and stream section [45, 98]. LW is also likely to be transported at the rising limb of floods and following the thalweg of the channel [16, 48, 68], while the presence of rootwad and branches was shown to significantly affect LW mobilisation and orientation, due to anchoring effects [2, 69].

Inertial measurement units for LW tracking

A recent study introduced inertial measurement units (IMUs), installed into scaled wooden dowels (SmartWood) for the quantification of LW dynamics from an isolated 'Lagrangian' perspective at a high temporal resolution in a laboratory setup [84]. IMUs typically provide accelerometer and gyroscope measurements in form of six-degree of freedom (6-DoF), or if additional readings from a magnetometer are considered nine-degree of freedom (9-DoF) sensor data. IMU-data were shown to provide essential information for the quantification of LW impact forces [86, 88], but also estimates of the initial orientation of LW [84]. The estimation of LW orientation requires sensor data integration and the use of sensor-fusion algorithms [50]. These processing steps were found to amplify errors when using 6-DoF sensor data (especially from low-budget sensors), severely affecting orientation estimates over longer periods of time (minutes, hours). Such errors are typically referred to as drift,

Spreitzer *et al. Environmental Sciences Europe*   (2024) 36:94

Page 3 of 22

and require the development of improved software algorithms for compensation [50, 84].

Sensor-fusion using IMU-data

Recent advances in sensor technology have led to a fast development of sensoementations across various fields or research interests, in particular for studies focusing on orientation estimation and object tracking. Sensor-fusion deals with the processing and combination of individual sensor data to increase the quality of output information. Typically, sensor-fusion is dealing with three-dimensional inertial measurements from accelerometer and gyroscope sensors (6-DoF IMU-data), which are combined in order to return a single measurement of orientation within the attitude and heading reference system (AHRS) that describes the orientation of a rigid object in three-dimensional space [60]. The sensor fusion algorithm is founded on the principle of gyroscopic integration for initial orientation estimates, while sensor data from accelerometer are needed for the reduction of drift (error of orientation estimates from sensor data integration) due to noise and biases [12, 51]. The most powerful technique for orientation estimation utilises Kalman filters or complementary filters [52]. The Kalman filter uses an angular derived approach to estimate orientation form gyroscope and accelerometer tilting, while complementary filters simply apply high- and low-pass filtering [34, 53]. Previous studies investigated the performance of both filters, with strongly varying conclusions. While Sabatini [75] and Islam et al. [39] stated an outstanding performance of the Kalman filter, Gui et al. [34] reported a slightly better performing complementary filter. Although Kalman filters were proven to yield highly accurate orientation estimates, they are complex to implement into algorithms and require large hardware resources, which result in higher computational expenses [39, 52], or even limited real-world applications due to the impracticability of the sensor-fusion algorithm [103]. Complementary filters may represent a good alternative, as they are simpler to implement, requiring lower processing power and allowing for the decoupling of yaw rotations from roll and pitch, that is not possible when using a Kalman filter approach. However, a big disadvantage of complementary filters is that they still remain widely unproven in freely available sensor-fusion algorithms to date [52].

Challenges and objectives

Although significant advances have been achieved in the tracking of LW in rivers, there is a lack of knowledge regarding LW movement dynamics at the field-scale for the short temporal scale (e.g., milli seconds, seconds, minutes) during floods due to limitations in applicable sensing techniques and processing algorithms. However, this knowledge is of great relevance for well-functioning LW retention as well as diversion structures and the mitigation of LW-related damage due to impacts and accumulations at critical instream infrastructure. The present study introduces and employs IMU-tagged logs (Smart-Wood) that improve the quantification of LW movement dynamics at a short temporal resolution. A sensor-fusion algorithm with complementary filters is used to estimate log-orientation from the recorded IMU-data, allowing for novel insights and the reconstruction of LW movement dynamics. The main objective of this study is to provide a better understanding of LW movement dynamics to inform decision-makers, engineers and researchers to maintain safety for critical instream infrastructure (e.g., bridges, weirs, hydropower plants) and human settlements. The robust design of LW retention and diversion structures requires fundamental knowledge of LW movement dynamics to guarantee functionality and to allow for a better control of wood depositional processes. Furthermore, if retention structures cannot be implemented, the safe bypassing and guiding of LW past critical cross-sections may be necessary and requires a profound understanding of LW movement dynamics during floods.

Methodology

IMU-tagged wood logs—SmartWood

At the Laboratory of Hydraulics, Hydrology and Glaciology (VAW) at ETH Zurich, IMUs have been developed to quantify movement dynamics of IMU-tagged wood logs (SmartWood) in rivers. The IMUs were built and assembled by a German company, Smart Solutions Technology [83]. Each IMU comprised an accelerometer, gyroscope, and magnetometer for measuring acceleration (g), angular velocity ($°·s^{-1}$) and magnetic flux (uT), respectively, and yielding a total of 9-DoF sensor data at a measuring frequency of 100 Hz. The IMUs were equipped with a processor for data-management and time synchronisation, an AA-battery (4.35 V, Li-ion cell), and an internal memory (8 MB). All of the individual components are situated within a waterproof (IP67) cylindrical PVC housing, measuring 105 mm in length and 25 mm in diameter (Fig. 1A), similar to the housing applied in a prior field study by [7]. In order to avoid the recording of stationary and "rocking in place" movement periods [64] and to safe battery lifetime and memory, the IMUs were programmed with a wake-up and sleep function based on a predefined acceleration threshold. Given the change in acceleration measurements was below ± 64 mg for 100 consecutive data points (1 s at 100 Hz), SmartWood entered a sleep-mode and woke up once acceleration exceeded ± 64 mg for a single data point (0.01 s at 100 Hz). Collected IMU-data of the present study are thus
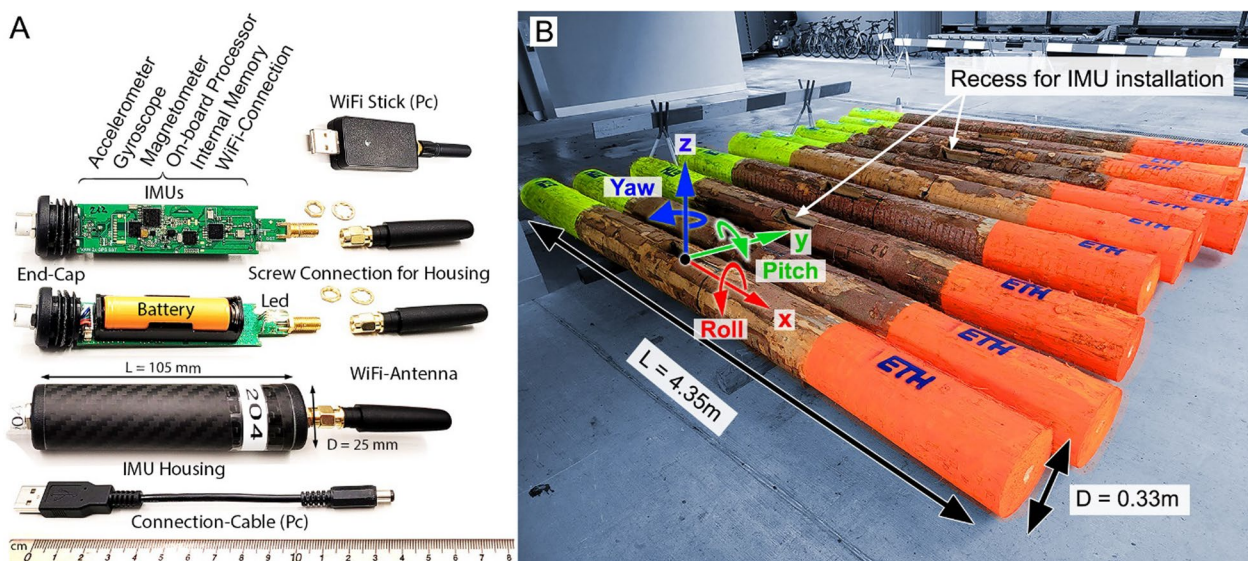
Fig. 1 Overview of the inertial measurement unit (IMU) and SmartWood for the experiments in the field

considered as discontinuous data, as data-gaps resulted from the IMU wake-up and sleep function. Another feature of the IMUs was the inclusion of a Wi-Fi transmitter with an external antenna that allowed for wireless communication and data transfer within a range of 100 m. To protect the IMU and antenna from mechanical damage during the experiments in rough stream environments, an external housing was developed to instal the IMU into the prototype wood logs (SmartWood). Each Smart-Wood-log was 4.35 m long with a mean diameter of 0.33 m and without rootwad or branches (Fig. 1B). The mass of the SmartWood-logs at the time of experiments was measured to 170 to 220 kg, yielding a density of roughly 500 kg·m^{-3}, which aligns with density estimates of LW from previous studies [15, 71, 84]. The rotational inertia around the x-axis is 2.7 kg·m^2, and 294 kg·m^2 for rotation around the y and z axes.

Orientation estimates from IMU-data

A freely available Python 'imufusion' package, provided by x-io Technologies [102], was used for the processing of orientation estimates in form of Euler angles from field-scale IMU-data. Although the present study collected data from all three sensor-units (accelerometer, gyroscope and magnetometer,9-DoF sensor data), the employed sensor-fusion algorithm by x-io Technologies [102] requires only 6-DoF sensor data from accelerometer and gyroscope for Euler angle estimates. The application of 6-DoF was previously shown to provide highly accurate orientation estimates from wearable IMUs [19, 28, 38]. Despite the consideration of 6-DoF sensor data for the computation of orientation estimates, the present

study still provides all 9-DoF sensor data, including data from magnetometer for the sake of completeness and discussion.

The 'imufusion' package, also known as an AHRS ("Sensor-fusion using IMU-data" section), such as initially developed by Madgwick [51], merges accelerometer and gyroscope data into a single orientation measurement in form of quaternions, while an improved complementary filter is used. A schematic flowchart of sensor-fusion algorithms with complementary filters has been presented by Nazarahari and Rouhani [61]. Quaternions represent the orientation of an object within a three-dimensional space and are typically expressed as a matrix or as more intuitively understandable Euler angles [50, 63]. All orientation estimates presented in this study refer to Euler angles and are defined as roll (rotation around the longitudinal x-axis), pitch (rotation around the lateral y-axis), and yaw (rotation around the vertical z-axis, Fig. 1B), allowing to derive movement behaviour of SmartWood during the experiments. In order to analyse the gained sensor data from field experiments, video footage was obtained via two UAVs (DJI Phantom 4 Pro), hand-held cameras from the banks (GoPro Hero 8), as well as from boats that were accompanying the SmartWood-logs.

Verification of IMU-data

To test and confirm the actual sensor movement with orientation measurements from the IMU, a verification procedure of trivial movement processes was required. The verification test was carried out with a handheld IMU and considered walking along a series of three

squares (side length, a ≈ 14 m) and circles (diameter, d ≈ 10 m) at the ETH Zurich Hönggerberg campus, close to the VAW test facility. Movement processes during the roughly 10-min-long verification procedure considered a combination of LW-like movements such as roll and yaw, in order to verify measured and reconstructed movement with observed movement. During all experiments the handheld IMU was carried in front of the body, about 1 m above the ground; only forward walking movement was tested. Results of these tests are presented in "Verification of IMU-data" section.

Field sites
A total of three rivers in Switzerland were selected for SmartWood experiments in the course of the present study. All experiments were conducted after heavy precipitation events in the summer of 2021, which has led to severe flooding in central Europe [44].

Limmat River
The first SmartWood experiment was conducted at the Limmat River during the falling limb of an annual flood at a discharge of roughly 200 $m^3 \cdot s^{-1}$ (peak discharge 280 $m^3 \cdot s^{-1}$). Lake Zurich provides the main source of the Limmat River, while < 10% of the base flow is supplied by the Sihl River, a tributary which was shown to carry large amounts of LW during floods in the past [79]. The Limmat River is 39 km long with an average gradient of 0.002, and empties into the Aare River [80]. The IMU-tagged log was released a short distance downstream of a diversion weir (47.409464 N, 8.444086 E), which ensures the water supply of the Werdbach River, a short tributary of the Limmat River situated about 10 km downstream of the city centre of Zurich and lake Zurich. Along the experimental test section at the Limmat River (Fig. 2A), a ferry dock is situated at the right bank (350 m from the point of release), while about 1 km further downstream, the Limmat River is impounded by the hydropower plant Dietikon, which is operated by the Electric Utilities of the Canton of Zurich (EKZ). The recovery of the IMU-tagged log was safely conducted via boat at the beginning of the impounded stream section. The average flow depth along the experimental test section was > 1 m and the average stream width was > 50 m.

Thur River
The second SmartWood experiment was conducted at the Thur River, also at the falling limb of an annual flood. The peak discharge of the flood (HQ_1 245 $m^3 \cdot s^{-1}$) occurred at night time, while the actual discharge rate at the time of the experiment the next morning was roughly 85 $m^3 \cdot s^{-1}$. The Thur River is 135 km long, with an average gradient of 0.013, emptying into the Rhine River [81]. The experimental test section (Fig. 2B) extends from the supply of SmartWood across of the campsite Gütighausen (47.587636 N, 8.739716 E), close to the town of Andelfingen in the Canton of Zurich, over a distance of roughly 4.2 km and through a series of three meanders to an accessible site on the right bank, where SmartWood was safely recovered via mobile crane. At the Thur River, the average flow depth along the experimental test section was > 1 m and the average stream width was > 40 m.

Grosse Melchaa River
The last experiment was performed at the Grosse Melchaa River, which is a small and steep channel in the Canton of Obwalden with a length of 18.5 km and an average gradient of 0.030, before emptying into the Lake Sarnersee [82]. After a rainfall event in the upper catchment, the up to 8 m wide channel showed a discharge of roughly 15 $m^3 \cdot s^{-1}$, at an average flow depth of about 0.5 m. The flow was characterised by macro-roughness stemming from very heterogeneous banks with large blocks on the bed and Froude Numbers up to 1.3, representing supercritical and highly turbulent flow conditions. The supply of SmartWood took place immediately upstream of a small bridge (46.803077 N, 8.284926 E), from the right bank (road) via rolling over a steep embankment and a roughly 2.5 m drop over a retention wall into the flooded channel. After a transport distance of just 140 m (Fig. 2C), the SmartWood log accumulated at big boulders and other LW in the channel centre, from where SmartWood was recovered via mobile crane.

Results
Verification of IMU-data
The IMU-data were successfully verified during pre-tests and the results are displayed in Fig. 3. The initial yaw orientation for the first side length of the first square was computed to be roughly 170° (a1 in Fig. 3). After walking along the first side length (a1) of the first square, a right turn (−90° yaw) was made which reduced the computed orientation estimate for yaw to roughly 80° for the second side length (a2) of the first square. The same initiated movement behaviour was followed for the third (a3) and fourth (a4) side length of the first square, resulting in a starting yaw orientation of again 170° for the first side length (a1) of the second square. During the third circuit around the square a −360° roll was conducted during translation along each side (Fig. 3), that has been accurately captured by the IMU and reconstructed via orientation estimates. After the fourth side length of the third square, no further right turn was made, yielding a final yaw orientation of roughly −100°, resulting in a drift in yaw orientation of approximately −10° for this short test. This drift is relatively small, however it still reflects the
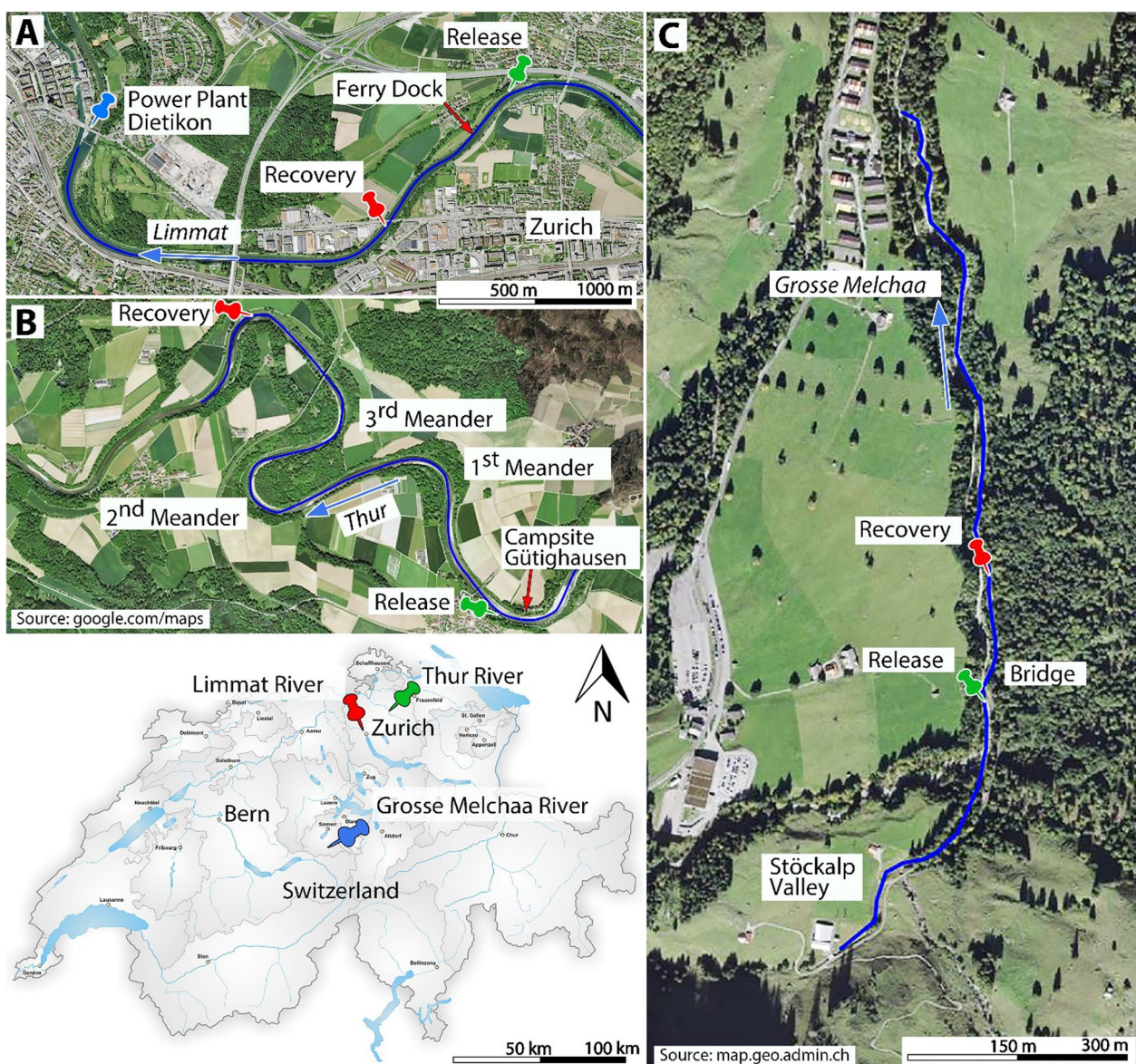
Fig. 2 Field sites of the conducted SmartWood experiments at the Limmat, Thur and Grosse Melchaa River in Switzerland (Map of Switzerland adapted from Tschubby [95])

limitation of only using 6-axis (i.e. accelerometer and gyroscope) data for sensor fusion and absolution orientation. If the absolute orientation (i.e. accurate yaw) of LW is needed during longer duration field deployments (i.e. for motion interpretation relative to bank absolute orientations) then more advanced 9-axis sensor fusion approaches are needed.

A further verification scenario considered the walking of three circles, starting with a yaw orientation of roughly 50° (Q1 of the first circle in Fig. 3). Again, the circle was walked clockwise (right turn), resulting in a negative yaw based on the IMU-orientation. After the first four

quarters (Q_1 to Q_4) of the first circle, the initial starting orientation was reached at a time of 660 s. A 5-s break was considered between each circle. The third circle considered additional clockwise roll ($-360°$) per semi-circle $Q_1 + Q_2$ as well as $Q_3 + Q_4$. At the end of Q_4 of the third circle, the initial starting orientation of 50° yaw was computed from the IMU-data.

IMU-results at the Limmat River

The recording of SmartWood at the Limmat River started from a perpendicular orientation with regard to the flow direction (0° Euler angles in Fig. 4). Raw
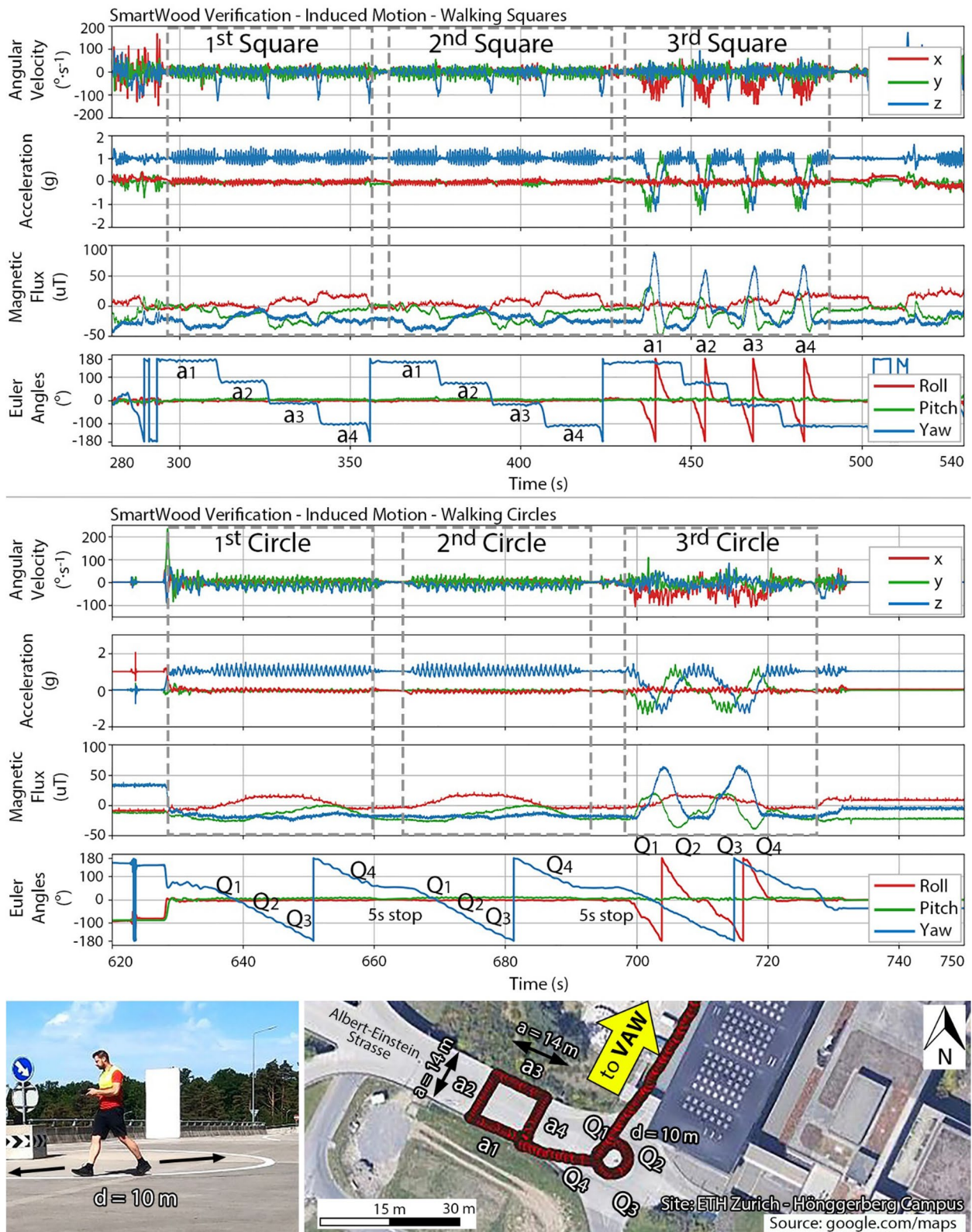
Spreitzer *et al. Environmental Sciences Europe*   (2024) 36:94

Page 7 of 22

Fig. 3 Verification of IMU-data and computed orientations (Euler angles) by means of walked squares and circles with a handheld IMU. The side length (*a*) of the square measured 14 m, while the diameter (*d*) of the circle measured 10 m. All data belong to the same dataset, while between each walk of the square and circle a 5-s stop was considered. The third square and circle included the rolling of the sensor per side and semicircle, respectively
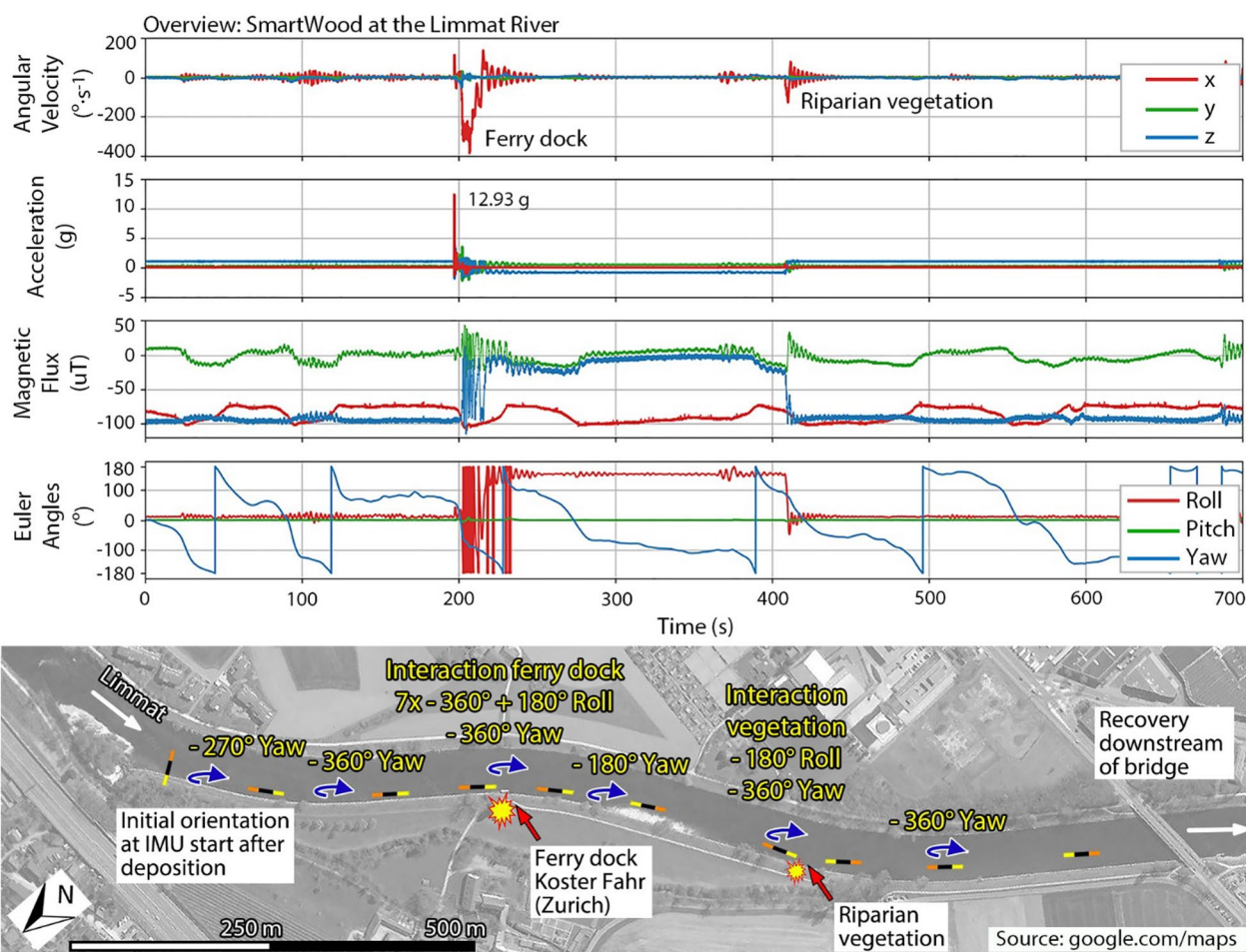
Fig. 4 Example of SmartWood movement dynamics at the Limmat River, showing interactions with a ferry dock (200 s) and riparian vegetation (410 s) during an annual flood

IMU-data do not indicate any significant movement dynamics, yet computed orientation estimates from the sensor raw data resulted negative yaw of $-270°$ during the first 60 s, with an additional $-360°$ yaw movement from 60 to 120 s. These results neatly align with observations in the field, where mobilisation occurred slowly along the right bank, involving multiple interactions with low riparian vegetation, and negative yaw of 1¾ rotations over the first two minutes of the experiment. Orientation estimates furthermore reveal that the IMU-tagged log was transported in parallel with the flow ($+90°$ yaw) for roughly 80 s, before raw data registered a significant impact ($+12.9$ g, x-axis) after roughly 200 s which triggered a notable angular velocity with a maximum rate of $-400°·s^{-1}$ around the longitudinal x-axis of the SmartWood-log. Video analyses from field observations confirm the reconstructed movement dynamics from raw IMU-data and Euler angles computation with great confidence, revealing an interaction

with the ferry dock at the right bank of the Limmat River (Fig. 4). Computed Euler angles indicate significant activity around the longitudinal axis of the SmartWood-log, requiring a separate and more detailed plot for analysis (Fig. 5). After the interaction with the ferry dock, the SmartWood-log was transported along the right bank and eventually interacted with large riparian vegetation, that jutted into the flooded channel, at roughly 410 s (Fig. 4). An impact was observed in the field (video footage), yet this impact is not visible at the large scale of acceleration data in Fig. 4, for which reason a closer look at the IMU-data is provided in Fig. 6, revealing a slight impact with a magnitude of $+0.58$ g. Both, computed IMU-data as well as visual observations in the field resulted in $-360°$ yaw and $-180°$ roll movement during the interaction of the log with the riparian vegetation. After seven minutes (420 s), the IMU-tagged log was transported further away from the right bank towards the channel centre for the first time,
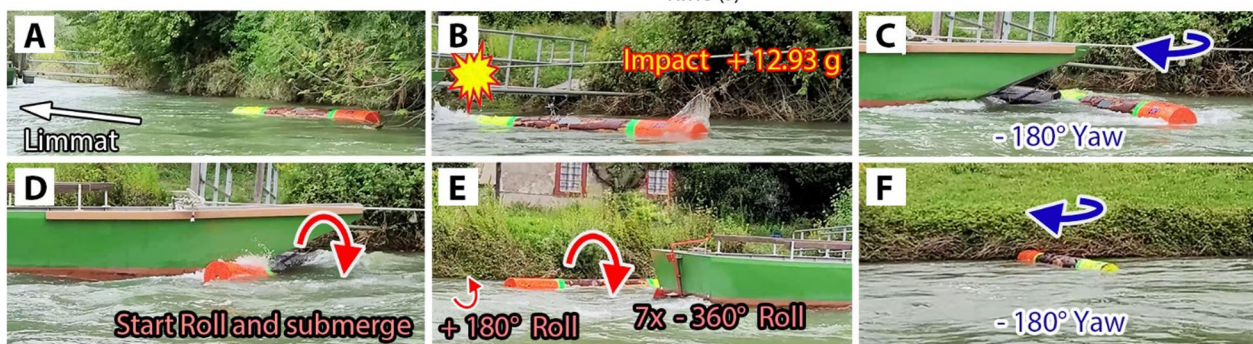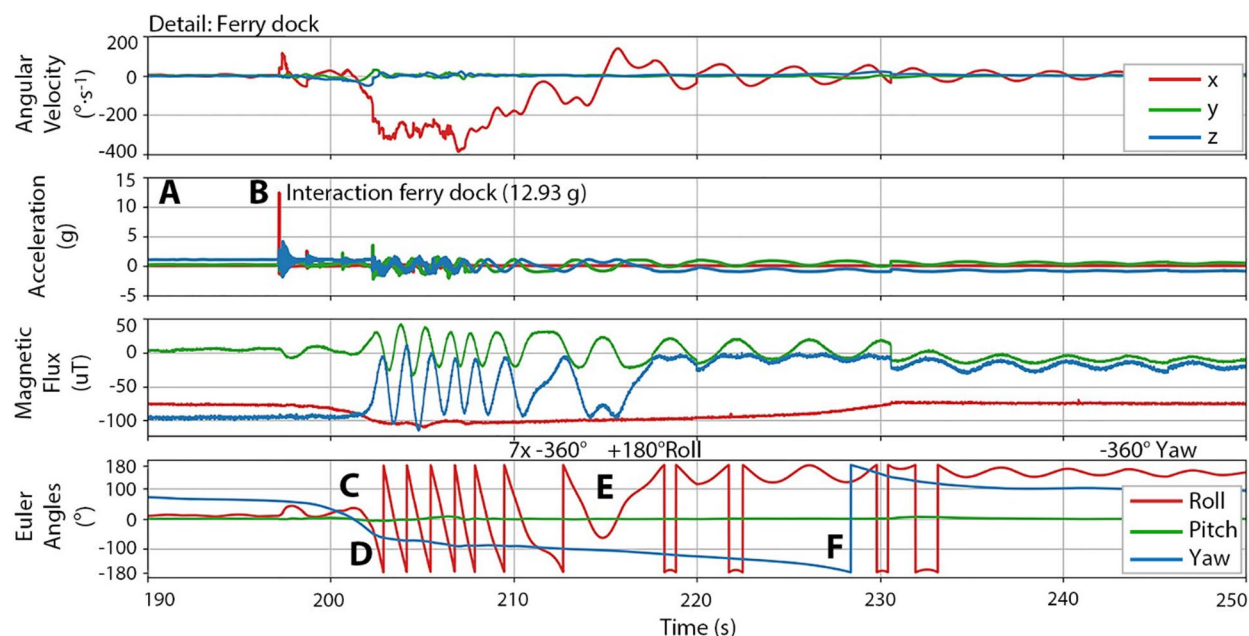
Fig. 5 Interaction of the IMU-tagged log with the ferry dock at the Limmat River

involving further negative yaw (−360°) before being recovered via boat downstream of the bridge (Fig. 4).

Figure 5 shows IMU raw data and Euler angles estimates that allow for a detailed analysis of LW dynamics during the interaction at the ferry dock. As the IMU-tagged log approached the ferry dock (Fig. 5A), sensor data are inconspicuous and orientation estimates show steady transport behaviour. The interaction of the log with the ferry dock was registered by the accelerometer with a peak magnitude of 12.93 g (Fig. 5B). Computed Euler angles revealed a subsequent negative yaw movement of −180° (Fig. 5C). Immediately after the −180° yaw movement, the log was transported beneath the ferry, involving a significant increase in angular velocity around the longitudinal x-axis (roll), before resurfacing between ferry and the right bank (Fig. 5D, E). Transport dynamics of the log beneath the ferry could not be observed via video footage, yet detailed Euler angles in Fig. 5D indicate seven full (−360°) roll rotations within 15 s (200 to 215

s), and a subsequent +180° roll movement (Fig. 5E). The extensive movement dynamics of the IMU-tagged log and transport beneath the ferry, is followed by a further 180° yaw in negative direction (Fig. 5F).

About 350 m downstream of the ferry dock, a branch from riparian vegetation jutted into the flooded channel, triggering an interaction with the SmartWood-log. As the SmartWood-log was approaching, an almost parallel orientation of the log with respect to the flow direction (−100° from starting orientation) was reconstructed via Euler angles, but also observed in the video footage (Fig. 6A). The interaction with some smaller riparian vegetation prior to the main event initiated slight seesaw roll and a −180° yaw movement (Fig. 6B, C). At a measuring time of 408 s, sensor raw-data revealed a slight impact with a magnitude of +0.58 g in longitudinal direction, at a time as the log interacted with the branch that was jutting into the flood waters (Fig. 6D). Although the impact magnitude was low, significant movement dynamics
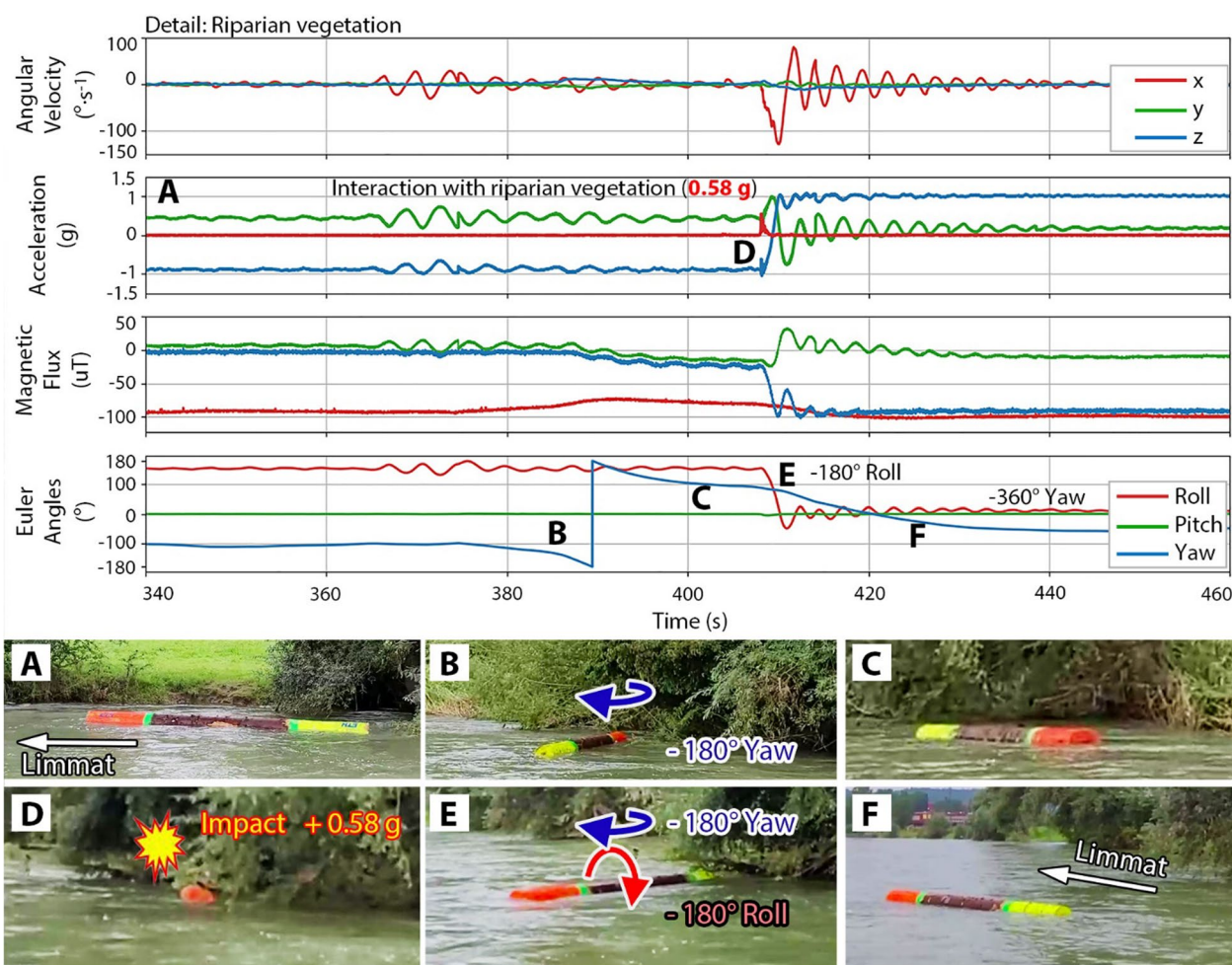
Fig. 6 Interaction of the IMU-tagged log with riparian vegetation at the Limmat River

were reconstructed from the interaction between the log with riparian vegetation, yielding orientation estimates of $-180°$ roll with an additional $-180°$ of yaw (Fig. 6E, F). According to observations during the experiment, the SmartWood-log was stopped by the branch, and experienced a ½ rotation around the longitudinal axis ($-180°$ roll) and another ½ rotation in clockwise direction around the vertical axis ($-180°$ yaw).

IMU-results at the Thur River

At the Thur River, the longest IMU-data set was acquired over a time period of almost 50 min from release to recovery. Figure 7 provides an overview of the gained raw data, computed Euler angles and a map with the schematic illustration of the roughly 4.2-km-long transport route according to observations from video footage. Immediately after the start of the IMU data record, results from Euler angle estimates indicate some major activity around the vertical axis (yaw, Fig. 8A). The registered

movement dynamics by the IMU originate from an artificially induced rotational motion via crane grapple before the actual release into the flooded Thur River, and are detailed for better analysis in Fig. 8. After the release of the SmartWood-log into the channel from the crane grapple, sensor data returned a significant roll movement (Fig. 8B), as well as a series of positive yaw rotations (Fig. 8B, C). Field observations revealed that the Smart-Wood-log was transported along the left bank while undergoing multiple rotations in counterclockwise direction around the vertical axis. About 1 km downstream of the release, the Thur River shifts from a stretched right bend into a left bend (1st Meander), at which the log moved from the left to the right shore (Fig. 7C). After the transit across the channel, the computed orientation estimates for the heading direction changed from positive to negative yaw movement, as video footage revealed. Eventually the IMU-tagged log impacted onto a boulder at the right bank (Fig. 7D), before continuing
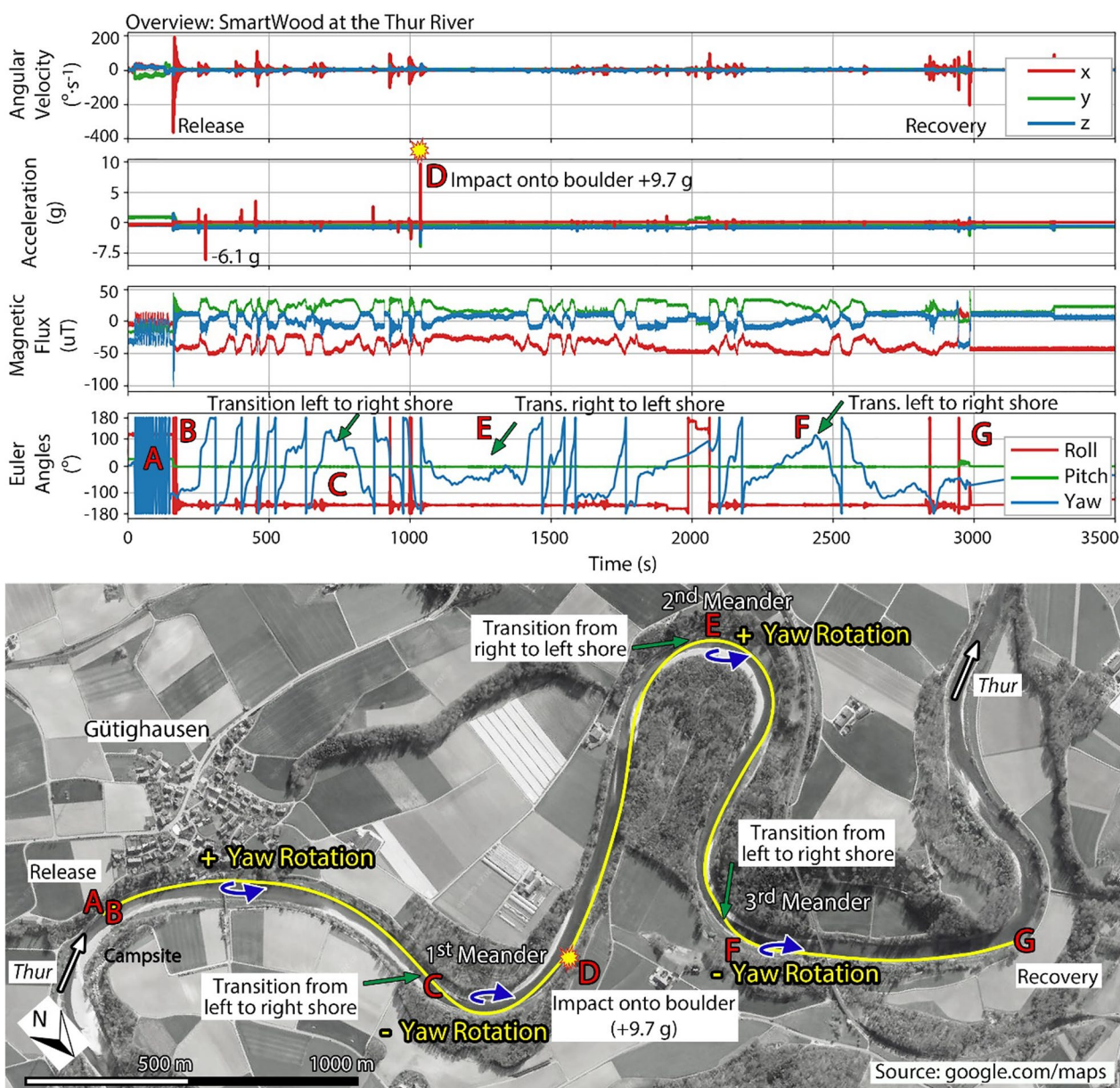
Fig. 7 Overview of IMU-data with a schematic illustration of the SmartWood transport route during an annual flood at the Thur River

transport along the right shore for about 1 km (Fig. 7D, E). At the 2nd Meander, the log moved from the right to left shore and was observed to be transported along the outer bend (Fig. 7E), while results from Euler angles estimates revealed a series of positive yaw movement dynamics within the measuring time of 1250 and 2250 s. Towards the end of the experiment, the IMU-tagged log moved a last time from the left to the right shore at the 3rd Meander (Fig. 7F), which resulted in negative yaw rotation, before the log has been recovered at the right shore (Fig. 7G). These yaw orientations and rotations are consistent with slower flow near the channel banks and faster flow near the centre of the river, resulting in rotation across the span of the SmartWood-log.

After the start of the IMU, the SmartWood-log was lifted from the left bank using a crane grapple, showing an initial orientation perpendicular to the flow direction (0° Euler angles, Fig. 8A). Prior to the release of the SmartWood-log into the Thur River, a significant yaw rotation ($-4050°$) has been computed from IMU-data due to the induced yaw rotation in clockwise direction around the crane grapple (Fig. 8B). The computed
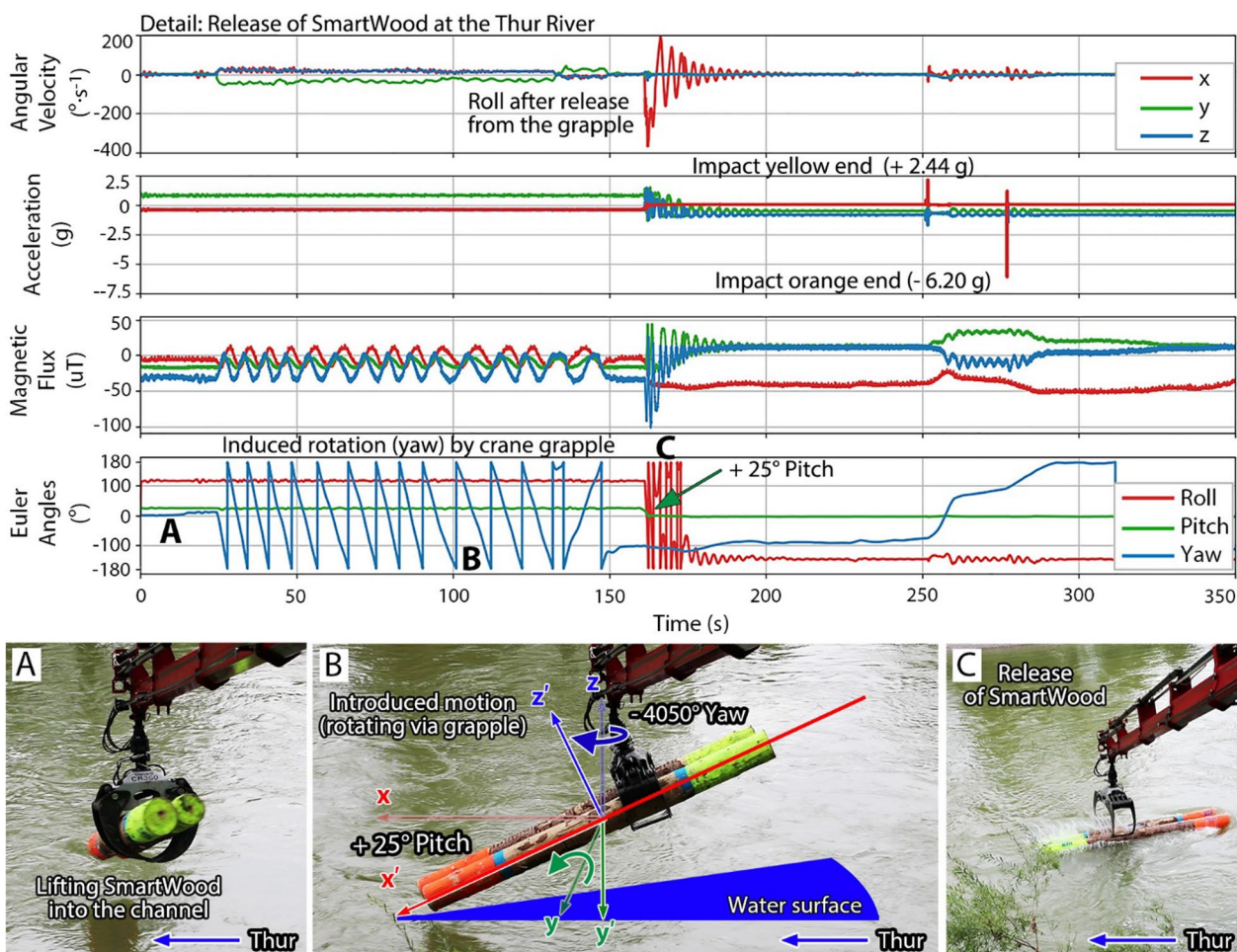
Fig. 8 The supply of SmartWood from the left bank at the Thur River started from a perpendicular orientation with respect to the flow direction (0° yaw orientation, **A**), undergoing a series of induced rotations (yaw) by the crane grapple (**B**), before being released into the flooded channel (**C**)

orientation estimates during the phase of induced motion furthermore revealed an inclination of roughly 25° pitch of the SmartWood-log while being held and rotated by the crane grapple (Fig. 8B). The release of the SmartWood-log parallel to the flow direction revealed a negative yaw orientation of −90°. With the opening of the grapple, a negative angular velocity around the longitudinal axis of the log was initiated, resulting a total of −630° roll (Fig. 8C).

Figure 9 details results during the first 20 min of the experiment at the Thur River and provides valuable insights into angular velocity, acceleration, and orientation estimates of LW movement dynamics during the falling limb of a flood. At the point of release, the computed Euler angles for yaw movement yielded −100°, representing the starting orientation of the IMU-tagged log at the Thur River (Fig. 9B). Field observations revealed that the IMU-tagged log was slowly mobilised and transported along the left bank, undergoing a series of seven full rotations in counterclockwise direction with respect to the flow direction at the current location of the log, resulting a total of +2520° yaw (7×360°), up to the point where the log moved from the left to the right bank. By contrast, over the first 700 s into the measurement (up to the point of transition of the log from the left to the right bank, Fig. 9C), computed Euler angles showed a total of five full yaw rotations plus an additional 230° yaw, resulting a total of +2030° yaw (5×360°+230°, Fig. 9B, C), and leaving a deficit of 490° yaw with regard to the observed yaw movement in the field. With the transit from the left to the right bank, orientation estimates for yaw changed from positive to negative direction in the Euler angles, and from counterclockwise to clockwise direction according to the observations in the field. At a time of roughly 1050 s, a major impact (+9.7 g) was registered by the accelerometer. From the point of transit across the channel (Fig. 9C) up to the major impact onto a boulder at the right bank at the exit of the 1st Meander
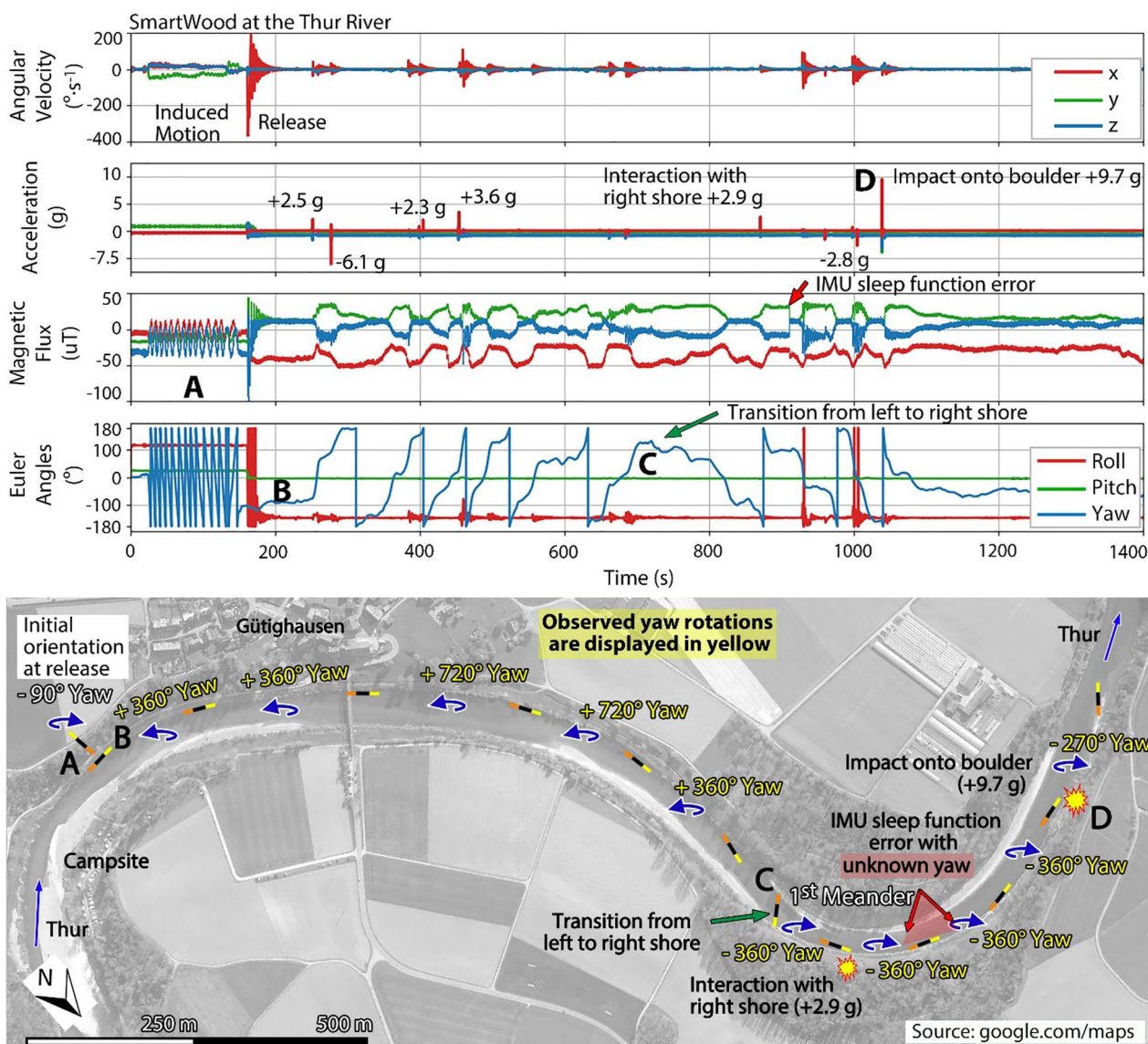
Fig. 9 Sectional analysis of IMU-tagged logs for orientation estimates at the meandering Thur River

(Fig. 9D), field observations revealed four full rotations into clockwise direction with respect to the flow direction and current location of the SmartWood-log, resulting in a total of $-1440°$ yaw $(4x-360°)$. At the same time, computed Euler angles showed a total of two full yaw rotations into negative direction plus an additional $-300°$ yaw, resulting in a total of $-1020°$ yaw $(2x-360°-300°$, Fig. 9C, D), and leaving a deficit of $420°$ yaw. In between the interaction with the right shore $(+2.9$ g, Fig. 9C) and the impact onto the boulder $(+9.7$ g, Fig. 9D), sensor data from magnetometer show an abrupt change in magnetic field strength at a time of roughly 900 s into the measurement, indicating an IMU sleep function error. Although

sensor data from magnetometer drop back to initial values, the effect on the computed orientation estimates was not detectable and remains unknown at this point.

IMU-results at the Grosse Melchaa River
The SmartWood experiment at the Grosse Melchaa River resulted in the capture of the highest movement dynamics of all experiments. IMU-data revealed high angular velocities of up to $750°\cdot s^{-1}$ and significant activity from the accelerometer. To prevent the IMU from entering the sleep-mode prior to release into the channel, the log had to be continuously rocked (Fig. 10A). The release of the SmartWood-log into the flooded Grosse Melchaa River
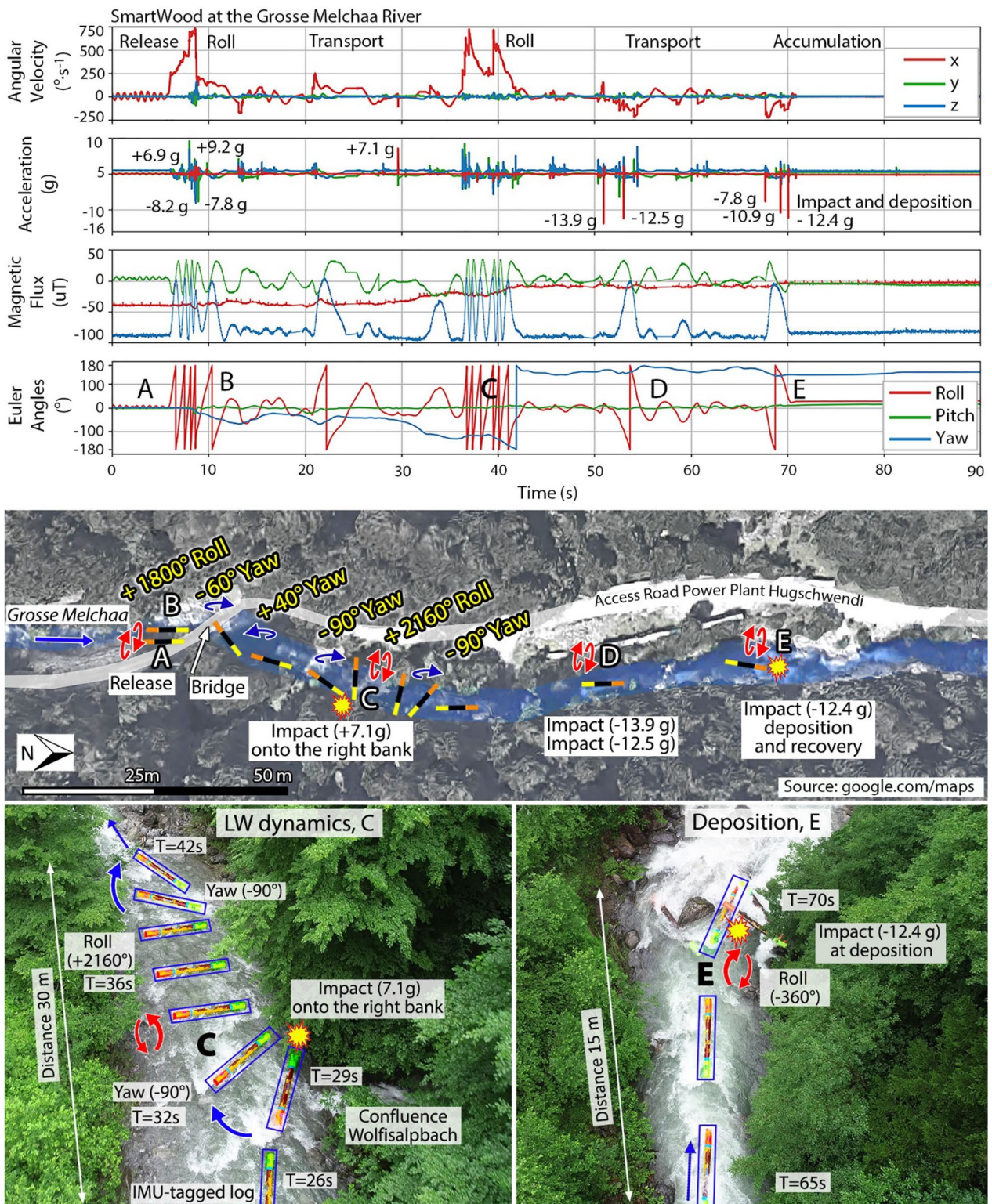
Fig. 10 Overview of IMU-data with a schematic illustration of the SmartWood transport route during a flood at the Grosse Melchaa River

was captured by an increase in angular velocity, as the log was rolling down the embankment for about 2 m, including lateral impacts after plunging over a roughly 2.5 m high retention wall into the channel. The acceleration readings for the feeding process ranged between -8.2 to $+9.2$ g, while the computation of orientation estimates resulted in 1800° roll (five rotations around the longitudinal axis, Fig. 10B). About 30 s after the start of the measurement, the IMU-tagged log interacted with a rock on the right bank, triggering an acceleration of $+7.1$ g along the longitudinal axis. Following the impact at the bank, raw IMU-data from gyroscope and accelerometer revealed a significant increase in angular velocity and acceleration peaks for both lateral axes. Results of the 'imufusion' algorithm show a $-180°$ yaw rotation as well as $+2160°$ of roll movement during the time of 29 to 42 s. Soon after the $-180°$ yaw rotation (Fig. 10C), sensor data from accelerometer registered two significant impacts (-13.9 and -12.5 g), as well as -360° roll (Fig. 10D). Towards the end of the experiment, a series of three impacts, ranging from -7.8 to -12.4 g, were measured as the SmartWood-log deposited alongside other logs at a big boulder in the centre of the channel (Fig. 10E). Computed orientation estimates revealed a further $-360°$ roll movement at deposition, which has also been observed in the field.

Discussion
Movement dynamics of LW during floods
The physical nature of LW dynamics is still not clearly understood to date for which reason an innovative sensing technique—SmartWood by Spreitzer et al. [84]—was tested for the first time in the field to quantify LW movement dynamics from an on-board perspective, that is not easily achievable with traditional techniques such as cameras [1, 47, 48] or RFID-tagged logs [49, 78]. Although SmartWood experiments were conducted during annual floods at the Limmat and Thur River, the registered movement dynamics were mostly monotonous and calm during transport along the tested stream sections. Several factors with regard to LW dimensions can be associated to the consistent and calm transport regime, such as the small relative log length of < 0.1, defined as the ratio of SmartWood length to average channel width Keller and Swanson [41], Bilby and Ward [10], Abbe et al. [3] as well as the small relative log diameter of < 0.3, defined as the ratio of SmartWood diameter to average flow depth Bilby [8], Mazzorana et al. [55]. Besides LW characteristics (e.g., log length, diameter, density), channel width and flow depth, also flow velocity and river sinuosity were previously found to represent main drivers for LW dynamics [15, 59, 66]. The present study observed calm flow conditions along the channel banks (with Froude

number Fr < < 1) and the channel centre (Fr < 1) at the Limmat and Thur River, which resulted in increased heading activity (yaw rotations) and reduced attitude (e.g., roll, pitch, impacts) dynamics of LW. By contrast, a low heading but increased attitude activity was measured at the smaller headwater stream at the Grosse Melchaa River. This can be explained due to the large relative log length and diameter ranging between 0.5 and 1.0, that reportedly promotes interactions of LW with the channel boundaries [5, 31] and consequently increases the complexity of LW movement dynamics. A diverse mix of interactions with rough channel elements (boulders, rocks) from the channel bed but also banks was observed and measured at the Grosse Melchaa river, due to the relatively high unit stream power at smaller headwater streams [21], which has a great ability to rapidly alter LW movement dynamics (Fig. 10). The gained results of the present study provide quantitative evidence that LW transport at lower flow depth and in more heterogeneous flow fields under supercritical conditions leads to higher stress on the wood logs due to the higher magnitude of impacts, rolling, and rotational dynamics, over just a short transport distance (Fig. 10). The actual measurement of increased movement dynamics and stress on LW elements within the present study links very well to observations of break-down processes of LW to smaller pieces in headwater streams [67, 90]. In detail, the IMU measurements registered significant roll movement at low flow depths (< LW diameter) from interactions with the channel bed during oblique or perpendicular orientation with respect to the flow (Fig. 10), matching with previous findings of transport dynamics of LW with similar density (500 kg·m^3) [22, 37, 71, 73]. It can be hypothesised that the interaction with the channel bed will be intensified for logs with increasing density [71]. In contrast, roll movement was measured after interactions with channel banks, riparian vegetation (Fig. 6), or objects (e.g., ferry dock at the Limmat River, Fig. 5) in deeper waters which occurred fully independent from the orientation of the LW piece. This study also confirms that the interaction potential of LW with riparian vegetation at piedmont rivers (e.g., Limmat and Thur River) may be increased during higher water levels, as previously stated by Tanaka and Yagisawa [94] and Gurnell [35]. The interaction of LW with riparian vegetation was found to induce impacts, roll, and yaw movement of SmartWood and altered the transport trajectory (Fig. 4). A transport trajectory of LW close to the thalweg [16, 48, 68], was observed at the Thur River, especially at the transition between the meanders (Fig. 7), but also at the Grosse Melchaa River, where the SmartWood-log was mainly transported by rapid currents (Fig. 10). On the other hand, a high frequency of interactions of SmartWood

with channel boundaries, in particular with the channel banks at the Limmat and Thur River, indicated that LW transport is governed by differences in local flow velocity such that the LW did not follow the primary flow path (thalweg). Turowski [96] elaborated the thalweg and gravel bedload path through meanders on the basis of studies by Dietrich and Smith [26] as well as Julien and Anthony [40]. Specifically, the deflection areas (zones along the outer bend of meanders, where bedload material interacts with the channel bank) for gravel bedload [96] were found to be similar to the areas with frequent interactions of LW with outer bend of stream meanders in the present study. This can be associated to secondary currents formed at the stream meanders guiding the LW towards the outer band due to elevated velocity at the water surface [11]. This mechanism has been leveraged by the design of LW retention racks placed parallel to the stream flow at outer bends [79]. Furthermore, LW was found to often transit through calm flow sections close to the banks at the Limmat and Thur River, in particular along straight channel sections (Fig. 4 and section E to F in Fig. 7), for which the transport trajectory of Smart-Wood shows consistency with the gravel bedload path elaborated by Turowski [96].

Orientation estimates of LW

Gained IMU-data provided the basis for the estimation of LW orientation from an on-board point of view [28, 32], that was previously identified to significantly affect LW mobilisation, transport, and deposition [15, 72, 84]. The conducted verification study and employed Python 'imu-fusion' package by x-io Technologies [102] yielded reliable and clearly comprehensible outcome to understand and reconstruct movement dynamics from IMU measurements (Fig. 3). Resulting Euler angles from the verification data-set showed insignificant drift in orientation estimates over short-medium timescales, such as previously reported by [84], and thus allowed for the use of the Python 'imufusion' package and the recorded IMU-data from field experiments to analyse LW movement dynamics. Computed Euler angles of the field tests yielded reliable and comprehensible orientation estimates for stream sections at the Limmat (Fig. 4) as well as Grosse Melchaa River (Fig. 10), which neatly aligned with actual movement dynamics from observations in the field. At the heavily meandering stream section of the Thur River, new insights into transport characteristics could be gained at a larger scale, even though challenges with drift and sensor-sleep phases arose for the detailed analysis of absolute orientation estimates from 6-DoF sensor data. An interaction of LW with the ferry dock at the Limmat River (Fig. 5) points out the clear advantage of IMU-data from an isolated 'Lagrangian' perspective compared to

traditionally applied observative methods for quantifying LW movement dynamics (e.g., impact magnitude) and orientation (e.g., roll and yaw) at high temporal resolution during visually obstructed transport phases, that could not be captured using solely visual or other remote sensing equipment.

A significant finding of the present field study was the measurement of consistent positive yaw movement along left stream banks, and consistent negative yaw movement along right stream banks (Figs. 4, 9 and 10). This can be associated to the cross-sectional distribution of surface velocity. Close to the banks the velocity gradients become more pronounced so that logs floating with transverse orientation experience different flow velocities and start to rotate. The consistency of the measured movement dynamics across all experimental test sections provided strong evidence that LW movement dynamics are following the principles of theoretical models and force-balance approaches from pioneer studies [15, 37]. The field measurements of this study enable to add additional information related to the heading orientation (positive/negative yaw direction), which has been missing in previous studies [15, 70]. Experiments at the Thur River demonstrated imposing movement dynamics, in particular heading orientations from Euler angles as the SmartWood-log passed through three meanders (Fig. 7). At the beginning of each meander, computed Euler angles revealed an apex in yaw orientation. This indicated that the SmartWood-log moved across the channel to the opposite bank due to secondary currents [48, 68, 96]. The positive yaw movement started with the interaction of the front end of the SmartWood-log with the left bank, while the rear end steadily moved towards the channel centre. This increased the oblique orientation of the SmartWood-log with respect to the flow and can affect the resulting drag force, which is governing for the log rotation [15, 73].

While IMU-data revealed new insights about rotational dynamics at the larger scale, a detailed analysis of computed orientations revealed large deviations of up to 490° from observed yaw movement for a series of seven rotations in counter clockwise direction (200 to 700 s in Fig. 9) and 420° from observed yaw movement for a series of four rotations in clockwise direction (700 to 1030 s in Fig. 9). One reason for the large deviations is linked to the manual yaw estimates, which were consistently obtained with regard to the flow direction at the current location of the LW piece [72]. Especially at heavily meandering stream sections (e.g., at the Thur River), the 'manual' yaw observations were found to overestimate each semi-rotation (180°) of yaw by up to 40° due to the curvature of the meander (Fig. 11). At the example of the heavily meandering Thur River, the successive overestimations from field observations may have
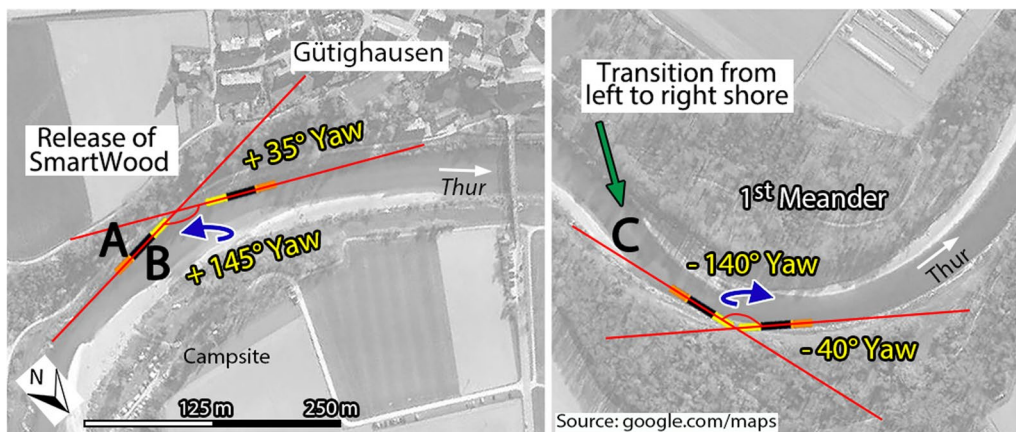
Fig. 11 Schematic illustration of the origin of the angular deficit due to observed yaw rotations with respect to the flow direction at the current location of the SmartWood-log, resulting up to 40° deficit per "180°" yaw rotation

resulted in significant deviations from computed orientation estimates, which strictly refer to the starting orientation, as no sensor data from magnetometer were used for global referencing [42, 52]. In addition, analysis of the IMU sleep function revealed an error at the Thur River, which became evident as an abrupt change of magnetic field strength in sensor data from magnetometer ($\approx$900 s in Fig. 9). Figure 12 shows that computed orientation estimates neglected "full 360°" rotations at meandering river reaches at a similar angular rate (up to 80° per full

yaw rotation) such as orientation estimates from field observations.

To obtain the LW transport trajectories, the estimation of the heading direction (yaw) from IMU-data is of particular interest [42]. By contrast, roll and pitch play a major role for the attitude of LW movement dynamics at the smaller scale such as LW interactions with channel boundaries, accumulations, or remobilisation [17, 84]. Due to gravitational measurements, the computed LW orientation in the horizontal plane (roll and pitch, e.g.,
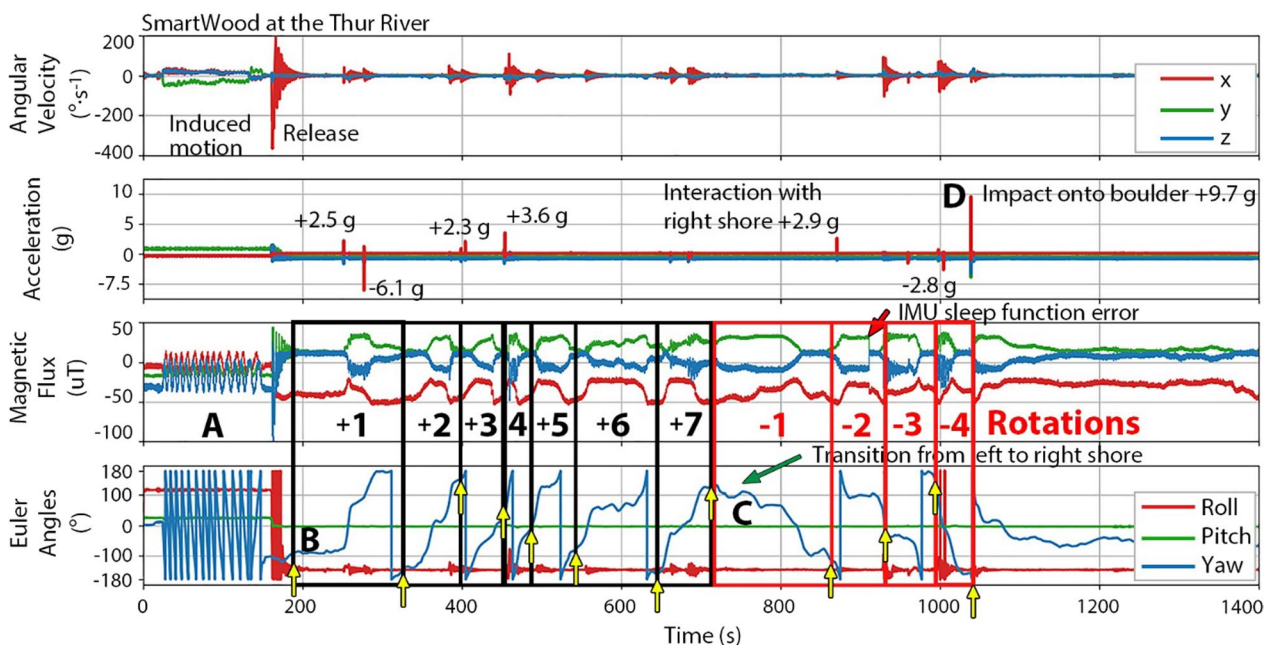

Fig. 12 Assessment of computed Euler angles estimates from 6DoF 'imufusion' algorithm with respect to magnetometer data from the Thur River, which are not considered in the currently employed 6DoF 'imufusion' algorithm. According to the sensor data from magnetometer, corresponding rotations, such as observed in the field can be linked to the Euler angle estimates

Spreitzer *et al. Environmental Sciences Europe*   (2024) 36:94

Page 18 of 22

Fig. 8) corresponded well to the actual movement of the SmartWood-log [52].

The implementation of additional sensor data from magnetometer is required to obtain precise estimations of the heading orientation (yaw) of LW in rivers. Using integration of angular velocities to estimate orientation is prone to drift over time, while sensor data from accelerometer solely return information about roll and pitch [52]. In addition, special emphasis should be put on the determination of the manually obtained orientation estimates in the field, which are intuitively determined with respect to the flow direction at the current location of the LW piece [72], rather than to the starting orientation [65].

Limitations and future requirements

Trivial inertial tracking systems for LW in rivers have not yet been developed. Currently, a compromise has to be made between the employed sensor units, the selected degrees of freedom (DoF), the amount of quantitative data, the employed sensor fusion algorithm, and the quality and accuracy of results from the chosen system. For example, magnetometer readings may be distorted by ferrous materials (e.g., bridges) and electromagnetic fields (e.g., power lines), while accelerometer data provide a mix of gravitational and non-gravitational acceleration that is not well-suited for orientation estimates in dynamic environments, and orientation estimates derived from gyroscope measurements are prone to drift over time [6, 51, 61]. The computed orientation estimates from 6-DoF provided novel insights into LW movement dynamics (e.g., positive/negative yaw movement at right/left stream banks, respectively). In particular, smaller SmartWood data-sets, such as the verification of an IMU (Fig. 3), and data-sets of almost straight stream sections at the Limmat (Fig. 4) and Grosse Melchaa River (Fig. 10) were shown to be capable of producing reliable and clearly comprehensible results that may be of great relevance for future LW studies that are focusing on details along a stream reach such as LW movement dynamics at critical instream infrastructures or retention and guiding structures [24, 80, 101]. However, the resulting differences in heading orientation of up to 490° yaw between computed 6-DoF and observed orientations at meandering rivers (Thur River, Fig. 9) currently restrict a detailed analysis of LW transport dynamics at the reach-scale and require two major improvements of the employed (i) IMUs and (ii) sensor fusion algorithm.

To further advance quantitative LW research at the field scale, the development of a robust IMU for the installation into LW pieces is needed. In order to precisely register movement dynamics in calm as well as highly dynamic stream environments, the upgraded IMU has to be equipped with sufficient battery lifetime and memory capacity, such as previously employed by Biggs et al. [7], for the continuous collection of data throughout an entire flood. The present study found that a wake-up and sleep function of the IMU may be counterproductive in terms of a source for errors. It can be recommended to remove this function, if not required for the autonomous start of measurements during the rising limb of floods or for the autonomous stop after deposition. The wake-up and sleep function was initially designed to prevent the recording of rocking in place scenarios [64, 84]. This makes it difficult to differentiate between real movement and wobbling and may affect the quality and outcome of orientation estimates, in particular in combination with the development of drift [50, 84]. The predefined threshold parameters for acceleration or angular velocity must be selected with care and should only consider the application of SmartWood within the specified stream reach, as flow conditions and transport dynamics may quickly vary [4, 100].

A case-specific sensor fusion algorithm is required for LW research, constraining possible movement regimes with the exclusion of physically impossible transport processes (e.g., upright transport of LW pieces or transport trajectories that are far off the water surface plane), and including additional data (e.g., GPS locations) that allow for a better reconstruction and analysis of LW movement dynamics [58, 87]. The majority of available algorithms, such as commercial sport tracking apps or inertial navigation systems, are strongly customised to suit a particular application, which is often following a specific movement behaviour [30, 46, 54], with the exclusion of unrealistic movement scenarios such as flipping or rolling. The implementation of additional sensor data (e.g., sensor data from magnetometer or GPS) into the sensor fusion algorithm may significantly improve the correlation between measured and observed heading orientations [52, 75] of LW with respect to the Earth's reference system (Fig. 12), rather than solely considering the starting orientation of the IMU-tagged log from 6-DoF sensor data. However, such sensor fusion codes lack maturity and often remain unproven in freely available sensor fusion algorithms [52], even though some 9-DoF sensors with integrated sensor fusion and absolute orientation have been available [13], trade-offs must be made with a decreased data sampling rate and increased power consumption compared to 6-DoF sensors as employed in the present study.

Conclusions

To maintain the beneficial aspects of wood in rivers and better control for LW-fluxes and accumulations during floods, an improved understanding of LW movement

Spreitzer *et al. Environmental Sciences Europe*   (2024) 36:94

Page 19 of 22

dynamics is required. Since Braudrick and Grant [15] addressed a major gap of quantitative data and models, a large number of studies have focused on the development of physical and numerical models to simulate LW movement dynamics during floods. However, the calibration and verification of these models require quantitative data of real-world LW movement dynamics, which are difficult to obtain and hence, are still missing to date.

The present study focused on the employment of prototype wood logs in combination with state-of-the-art IMUs (SmartWood) to quantify LW movement dynamics during floods from a fully isolated 'Lagrangian' point of view. This approach has shown to have great advantages over traditionally applied observative methods such as cameras or RFID tags. The introduced SmartWood method yielded the collection of innovative field-scale data along three tested stream sections in Switzerland. Specifically, we obtained highly resolved individual transport details over long transport distances which are often not detectable by visual sensing techniques (e.g., submerged LW transport after the interaction with a ferry dock at the Limmat River). Although the acquired data of the present study are discontinuous, collected IMU-data and computed orientation estimates showed great consistency with actual observations in the field (video footage), allowed for the comprehensible analysis of LW transport through short key sections as well as at critical-cross sections, and granted novel insights into LW movement dynamics during floods. Orientation estimates from IMU-data revealed consistent positive yaw movement during LW transport along the left stream bank and negative yaw movement while being transported along right stream banks. Quantitative data furthermore indicated that transport dynamics are more complex and of higher magnitude at the smaller headwater stream than at flooded piedmont rivers. This can be related to the ratio between the SmartWood dimensions to the river dimensions (i.e. relative log length and diameter). Significant deviations became evident between computed orientation estimates and observed orientations along a heavily meandering stream section, while reliable and comprehensible orientation estimates resulted for straight stream sections. The gained results are of great relevance to validate and improve numerical models [65, 74], and to identify an optimal location for LW retention and guiding structures [79] or other engineered instream structures (e.g., engineered log jams) in the course of river restoration projects [62]. Going forward, the introduced SmartWood-method requires further development in order to (i) generate continuous data of LW movement dynamics over longer periods of time; (ii) employ 9-DoF IMU-data that include sensor data from the magnetometer; to (iii) generate orientation estimates with regard to a global (earth) reference system, that will further improve the quality of quantitative data and analysis of LW movement dynamics at the field scale.

Author contributions
Dr. Gabriel Spreitzer: funding acquisition. MSCA-IF & BAFU; conceptual design and elaboration of methodology; planning, organisation and coordination of field experiments; data acquisition, processing and analysis; Writing. Dr. Isabella Schalko: funding acquisition BAFU; support in data acquisition at the Limmat River, discussion and internal review. Prof. Dr. Robert M. Boes: funding acquisition BAFU; discussion and internal review. Dr. Volker Weitbrecht: funding acquisition BAFU; support in data acquisition at the Limmat and Thur Rivers, discussion and internal review.

Data availability
The datasets used and/or analysed during the current study are available from the first author on reasonable request.

Declarations

Consent for publication
Not applicable.

Competing interests
The authors declare that they have no competing interests.

Author details
[1]Laboratory of Hydraulics, Hydrology and Glaciology (VAW), ETH Zurich, CH-8093 Zurich, Switzerland. [2]Swiss Federal Research Institute WSL, CH-8903 Birmensdorf, Switzerland.

References
1. Aarnink J, Ruiz-Villanueva V, Vuaridel M (2022) Machine learning and RFID-based large wood tracking in rivers. EGU General Assembly 2022.
2. Abbe TB, Montgomery DR (1996) Large woody debris jams, channel hydraulics and habitat formation in large rivers. Regul River 12(2–3):201–221. https://doi.org/10.1002/(Sici)1099-1646(199603)12:2/3%3c201::Aid-Rrr390%3e3.3.Co;2-1
3. Abbe TB, Montgomery DR, Fetherston KL, McClure E (1993) A process-based classification of woody debris in a fluvial network: preliminary analysis of the Queets River. Washington EOS Transactions AGU 74:296

4. Sawaf AL et al (2020) Assessment of mountain river streamflow patterns and flood events using information and complexity measures. J Hydrol. https://doi.org/10.1016/j.jhydrol.2020.125508

5. Berg N, Carlson A, Azuma D (1998) Function and dynamics of woody debris in stream reaches in the central Sierra Nevada, California. Can J Fish Aquat Sci 55(8):1807–1820. https://doi.org/10.1139/f98-064

6. Bhardwaj R, Kumar N, Kumar V (2017) Errors in micro-electro-mechanical systems inertial measurement and a review on present practices of error modelling. Trans Inst Meas Control 40(9):2843–2854. https://doi.org/10.1177/0142331217708237

7. Biggs H, Starr A, Smith B, de Lima S, Sykes J, Haddadchi A, Smart G, Hicks M (2022) Kinematic loggers-development of rugged sensors and recovery systems for field measurements of stone rolling dynamics and impact accelerations during floods. Sensors (Basel). https://doi.org/10.3390/s22031013

8. BILBY R (1984) Removal of woody debris may affect stream channel stability. J Forest 82:609–613

9. Bilby R (1985) Influence on stream size on the function and characteristics of large organic debris. West Coast Meeting of the National Council of the Paper Industry for Air and Stream Improvement, 1–14.

10. Bilby RE, Ward JW (1989) Changes in characteristics and function of woody debris with increasing size of streams in Western Washington. Trans Am Fish Soc 118(4):368–378. https://doi.org/10.1577/1548-8659(1989)118%3c0368:CICAFO%3e2.3.CO;2

11. Blanckaert K, de Vriend HJ (2004) Secondary flow in sharp open-channel bends. J Fluid Mech 498:353–380. https://doi.org/10.1017/s0022112003006979

12. Bortz J (1971) A New Mathematical Formulation for Strapdown Inertial Navigation. Ieee Transactions On Aerospace And Electronic Systems, AES-7, NO. I. https://ieeexplore.ieee.org/stamp/stamp.jsp?tp=&arnumber=4103660

13. BOSCH (2024) Smart sensor: BNO055 - Integrated MCU + flash. Integrated sensor fusion. https://www.bosch-sensortec.com/products/smart-sensor-systems/bno055/

14. Boucher Y, Arseneault D, Sirois L (2009) Logging history (1820–2000) of a heavily exploited southern boreal forest landscape: Insights from sunken logs and forestry maps. For Ecol Manage 258(7):1359–1368. https://doi.org/10.1016/j.foreco.2009.06.037

15. Braudrick CA, Grant GE (2000) When do logs move in rivers? Water Resour Res 36(2):571–583. https://doi.org/10.1029/1999wr900290

16. Braudrick CA, Grant GE (2001) Transport and deposition of large woody debris in streams: a flume experiment. Geomorphology 41(4):263–283. https://doi.org/10.1016/S0169-555x(01)00058-7

17. Braudrick CA, Grant GE, Ishikawa Y, Ikeda H (1997) Dynamics of wood transport in streams—a flume experiment. Earth Surf Process Landf 22(7):669–683. https://doi.org/10.1002/(SICI)1096-9837(199707)22:7%3c669::AID-ESP740%3e3.0.CO;2-L

18. Burns J (1972) Some effects of logging and associated road construction on Northern California Streams. Trans Am Fish Soc 101(1):17

19. Camomilla V, Bergamini E, Fantozzi S, Vannozzi G (2018) Trends supporting the in-field use of wearable inertial sensors for sport performance evaluation: a systematic review. Sensors (Basel). https://doi.org/10.3390/s18030873

20. Cave M, Davies N, Langford J (2017) Cyclone cook slash investigation 2017 report. Gisborne district council—land and soil environmental services and protection, 121. https://www.gdc.govt.nz/_data/assets/pdf_file/0013/10408/cyclone-cook-slash-investigation-2017-report.pdf

21. Chen S-C, Chao Y-C, Chan H-C (2013) Typhoon-dominated influence on wood debris distribution and transportation in a high gradient headwater catchment. J Mt Sci 10(4):509–521. https://doi.org/10.1007/s11629-013-2741-2

22. Chen S-C, Tfwala SS, Wang C-R, Kuo Y-M, Chao Y-C (2019) Incipient motion of large wood in river channels considering log density and orientation. J Hydraul Res 58(3):489–502. https://doi.org/10.1080/00221686.2019.1625816

23. Comiti F, Andreoli A, Mao L, Lenzi MA (2008) Wood storage in three mountain streams of the Southern Andes and its hydro-morphological effects. Earth Surf Process Landf 33(2):244–262. https://doi.org/10.1002/esp.1541

24. Comiti F, D'agostino V, Moser M, Lenzi Ma, Bettella F, Dell'agnese A, Rigon E, Gius S, Mazzorana B. (2012) Preventing wood-related hazards

in mountain basins from wood load estimation to designing retention structures. 12th Congress INTERPRAEVENT 2012 – Grenoble / France, 12, 12. http://www.interpraevent.at/palm-cms/upload_files/Publikationen/Tagungsbeitraege/2012_2_651.pdf

25. Cormack RGH (1949) A study of trout streamside cover in logged-over and undisturbed virgin spruce woods. Can J Res C 27(3):78–000. https://doi.org/10.1139/cjr49c-007

26. Dietrich WE, Smith JD (1984) Bed load transport in a river meander. Water Resour Res 20(10):1355–1380. https://doi.org/10.1029/WR020i010p01355

27. Europeana Foundation (2019) Taming the rivers—Log driving in Sweden and Finland. Europeana Foundation. https://www.europeana.eu/de/blog/taming-the-rivers-log-driving-in-sweden-and-finland

28. Falbriard M, Meyer F, Mariani B, Millet GP, Aminian K (2020) Drift-free foot orientation estimation in running using wearable IMU. Front Bioeng Biotechnol 8:65. https://doi.org/10.3389/fbioe.2020.00065

29. Fan J, Huang G (2020) Evaluation of flood risk management in japan through a recent case. Sustainability. https://doi.org/10.3390/su12135357

30. Filippeschi A, Schmitz N, Miezal M, Bleser G, Ruffaldi E, Stricker D (2017) Survey of motion tracking methods based on inertial sensors: a focus on upper limb human motion. Sensors (Basel). https://doi.org/10.3390/s17061257

31. Galia T, Tichavský R, Škarpich V, Šilhán K (2018) Characteristics of large wood in a headwater channel after an extraordinary event: the roles of transport agents and check dams. CATENA 165:537–550. https://doi.org/10.1016/j.catena.2018.03.010

32. Gonzalez-Alonso J, Oviedo-Pastor D, Aguado HJ, Diaz-Pernas FJ, Gonzalez-Ortega D, Martinez-Zarzuela M (2021) Custom IMU-based wearable system for robust 2.4 GHz wireless human body parts orientation tracking and 3D movement visualization on an avatar. Sensors (Basel). https://doi.org/10.3390/s21196642

33. Gschnitzer T, Gems B, Mazzorana B, Aufleger M (2017) Towards a robust assessment of bridge clogging processes in flood risk management. Geomorphology 279:128–140. https://doi.org/10.1016/j.geomorph.2016.11.002

34. Gui Pf, Tang Lq, Mukhopadhyay S (2015) MEMS based IMU for tilting measurement: comparison of complementary and Kalman filter based data fusion. C Ind Elect Appl, 1998–2003. https://ieeexplore.ieee.org/stamp/stamp.jsp?tp=&arnumber=7334442

35. Gurnell AM (2013) Wood in fluvial systems. Shroder, J. (Editorin Chief), Wohl, E. (Ed.), Treatise on geomorphology. Academic Press, San Diego, CA, 9(FluvialGeomorphology), 163–188. https://doi.org/10.1016/b978-0-12-374739-6.00236-0

36. Haehnel RB, Daly SF (2004) Maximum impact force of woody debris on floodplain structures. J Hydraul Eng 130(2):112–120. https://doi.org/10.1061/ASCE/0733-9429/2004/130:2/112

37. Haga H, Kumagai TO, Otsuki K, Ogawa S (2002) Transport and retention of coarse woody debris in mountain streams: an in situ field experiment of log transport and a field survey of coarse woody debris distribution. Water Resour Res. https://doi.org/10.1029/2001wr001123

38. ILUK A (2023) Flight Controller as a Low-Cost IMU Sensor for Human Motion Measurement. Sensors (Basel). https://doi.org/10.3390/s23042342

39. Islam T, Islam MS, Shajid-Ul-Mahmud M, Hossam-E-Haider M (2017) Comparison of complementary and Kalman filter based data fusion for attitude heading reference system. https://doi.org/10.1063/1.5018520

40. Julien PY, Anthony DJ (2002) Bed load motion and grain sorting in a meandering stream. J Hydraul Res 40(2):125–133. https://doi.org/10.1080/00221680209499855

41. Keller E, Swanson FJ (1979) Effects of large organic material on channel form and fluvial processes. Earth Surf Process Landf 4:361–380

42. Laidig D, Seel T (2023) VQF: Highly accurate IMU orientation estimation with bias estimation and magnetic disturbance rejection. Inf Fusion 91:187–204. https://doi.org/10.1016/j.inffus.2022.10.014

43. Lange D, Bezzola GR (2006) Schwemmholz - Probleme und Lösungsansätze. VAW-Mitteilung 188 (H.-E. Minor, Hrsg.), Versuchsanstalt für Wasserbau, Hydrologie und Glaziologie (VAW), ETH Zürich. https://ethz.ch/content/dam/ethz/special-interest/baug/vaw/vaw-dam/documents/das-institut/mitteilungen/2000-2009/188.pdf

Spreitzer *et al. Environmental Sciences Europe*   (2024) 36:94

Page 21 of 22

44. Lehmkuhl F, Schüttrumpf H, Schwarzbauer J, Brüll C, Dietze M, Letmathe P, Völker C, Hollert H (2022) Assessment of the 2021 summer flood in Central Europe. Environ Sci Eur. https://doi.org/10.1186/s12302-022-00685-1

45. Lienkaemper GW, Swanson FJ (1987) Dynamics of large woody debris in streams in old-growth Douglas-fir forests. Can j For Res 17:150–156

46. Longo UG, de Salvatore S, Sassi M, Carnevale A, de Luca G, Denaro V (2022) Motion tracking algorithms based on wearable inertial sensor: a focus on shoulder. Electronics. https://doi.org/10.3390/electronics11111741

47. Lyn Da, Cooper T, Yi Y, Sinha R, Rao R (2003) Debris accumulation at bridge crossings, laboratory and field studies. TRB Subject Code: 25–1 Publication No.: FHWA/IN/JTRP-2003/10, SPR-2478.

48. Macvicar B, Piégay H (2012) Implementation and validation of video monitoring for wood budgeting in a wandering piedmont river, the Ain River (France). Earth Surf Process Landf 37(12):1272–1289. https://doi.org/10.1002/esp.3240

49. Macvicar BJ, Piegay H, Henderson A, Comiti F, Oberlin C, Pecorari E (2009) Quantifying the temporal dynamics of wood in large rivers: field trials of wood surveying, dating, tracking, and monitoring techniques. Earth Surf Process Landf 34(15):2031–2046. https://doi.org/10.1002/esp.1888

50. Madgwick SO, Harrison AJ, Vaidyanathan A (2011) Estimation of IMU and MARG orientation using a gradient descent algorithm. IEEE Int Conf Rehabil Robot 2011:5975346. https://doi.org/10.1109/ICORR.2011.5975346

51. Madgwick SOH (2014) AHRS algorithms and calibration solutions to facilitate new applications using low-cost MEMS The University of Bristol. https://ethos.bl.uk/OrderDetails.do?uin=uk.bl.ethos.681552

52. Madgwick SOH, Wilson S, Turk R, Burridge J, Kapatos C, Vaidyanathan R (2020) An extended complementary filter for full-body MARG orientation estimation. IEEE/ASME Trans Mechatron 25(4):2054–2064. https://doi.org/10.1109/tmech.2020.2992296

53. Mahony R, Hamel T, Pflimlin J-M (2008) Nonlinear complementary filters on the special orthogonal group. IEEE Trans Autom Control 53(5):1203–1218. https://doi.org/10.1109/tac.2008.923738

54. MARIN F (2020) Human and animal motion tracking using inertial sensors. Sensors (Basel). https://doi.org/10.3390/s20216074

55. Mazzorana B, Hübl J, Zischg A, Largiader A (2011) Modelling woody material transport and deposition in alpine rivers. Nat Hazards 56(2):425–449. https://doi.org/10.1007/s11069-009-9492-y

56. Meehan WR, Farr WA, Bishop DM, Patric JH (1969) Some effects of clearcutting on salmon habitat on two southeastern Alaska streams. USDA Forest Service General Technical Report, PNW-82(Pacific Northwest For. and Range Exp. Stn., Portland, Oregon).

57. Melville BW, Dongol MS (1992) Bridge pier scour with debris accumulation. J Hydraul Eng 118(9):1306–1310

58. Mortensen RM, Reinhardt S, Hjønnevåg ME, Wilson RP, Rosell F (2021) Aquatic habitat use in a semi-aquatic mammal: the Eurasian beaver. Anim Biotelemetry. https://doi.org/10.1186/s40317-021-00259-7

59. Nakamura F, Swanson FJ (1994) Distribution of coarse woody debris in a mountain stream, western cascade range. Oregon Can J For Res 24(12):2395–2403. https://doi.org/10.1139/x94-309

60. Navidi N, Landry R (2021) A new perspective on low-cost MEMS-based AHRS determination. Sensors (Basel). https://doi.org/10.3390/s21041383

61. Nazarahari M, Rouhani H (2021) 40 years of sensor fusion for orientation tracking via magnetic and inertial measurement units: methods, lessons learned, and future challenges. Inf Fusion 68:67–84. https://doi.org/10.1016/j.inffus.2020.10.018

62. Neuhaus V, Mende M (2021) Engineered large wood structures in stream restoration projects in switzerland: practice-based experiences. Water. https://doi.org/10.3390/w13182520

63. Ohkami Y (2001) Spacecraft dynamics - ll.D euler angles. Encyclopedia of physical science and technology, Third Edition.

64. Olinde L, Johnson JPL (2015) Using RFID and accelerometer-embedded tracers to measure probabilities of bed load transport, step length, and rest times in mountain stream. Water Resour Res 51(9):7572–7589. https://doi.org/10.1002/2014WR016120

65. Persi E, Meninno S, Petaccia G, Sibilla S, Armanini A (2022) Modeling large wood transport in semi-congested regime with multiple entry points. Water. https://doi.org/10.3390/w14030421

66. Persi E, Petaccia G, Sibilla S (2017) Large wood transport modelling by a coupled Eulerian-Lagrangian approach. Nat Hazards 91:59–74. https://doi.org/10.1007/s11069-017-2891-6

67. Phillips C, Marden M, Basher LR (2018) Geomorphology and forest management in New Zealand's erodible steeplands: an overview. Geomorphology 307:107–121. https://doi.org/10.1016/j.geomorph.2017.07.031

68. Ravazzolo D, Mao L, Picco L, Lenzi MA (2015) Tracking log displacement during floods in the Tagliamento River using RFID and GPS tracker devices. Geomorphology 228:226–233. https://doi.org/10.1016/j.geomorph.2014.09.012

69. Ravazzolo D, Spreitzer G, Tunnicliffe J, Friedrich H (2022) The effect of large wood accumulations with rootwads on local geomorphic changes. Water Resour Res. https://doi.org/10.1029/2021WR031403

70. Ruiz-Villanueva V, Mazzorana B, Bladé E, Bürkli L, Iribarren-Anacona P, Mao L, Nakamura F, Ravazzolo D, Rickenmann D, Sanz-Ramos M, Stoffel M, Wohl E (2019) Characterization of wood-laden flows in rivers. Earth Surf Process Landf 44:1694–1709. https://doi.org/10.1002/esp.4603

71. Ruiz-Villanueva V, Piegay H, Gaertner V, Perret F, Stoffel M (2016) Wood density and moisture sorption and its influence on large wood mobility in rivers. CATENA 140:182–194. https://doi.org/10.1016/j.catena.2016.02.001

72. Ruiz-Villanueva V, Piegay H, Gurnell AA, Marston RA, Stoffel M (2016) Recent advances quantifying the large wood dynamics in river basins: New methods and remaining challenges. Rev Geophys 54(3):611–652. https://doi.org/10.1002/2015rg000514

73. Ruiz-Villanueva V, Wyżga B, Zawiejska J, Hajdukiewicz M, Stoffel M (2016) Factors controlling large-wood transport in a mountain river. Geomorphology 272:21–31. https://doi.org/10.1016/j.geomorph.2015.04.004

74. Ruiz-Villanueva V, Gamberini C, Bladé E, Stoffel M, Bertoldi W (2020) Numerical modeling of instream wood transport, deposition, and accumulation in braided morphologies under unsteady conditions: sensitivity and high-resolution quantitative model validation. Water Resour Res. https://doi.org/10.1029/2019wr026221

75. SABATINI AM (2006) Quaternion-based extended Kalman filter for determining orientation by inertial and magnetic sensing. IEEE Trans Biomed Eng 53(7):1346–1356. https://doi.org/10.1109/TBME.2006.875664

76. Schalko I (2018) Modeling hazards related to large wood in rivers VAW-Mitteilung 249 (R. Boes, Hrsg.), Versuchsanstalt für Wasserbau, Hydrologie und Glaziologie (VAW), ETH Zürich. doi:https://doi.org/10.3929/ethz-b-000293084

77. Schalko I, Wohl E, Nepf HM (2021) Flow and wake characteristics associated with large wood to inform river restoration. Sci Rep 11(1):8644. https://doi.org/10.1038/s41598-021-87892-7

78. Schenk ER, Moulin B, Hupp CR, Richter JM (2014) Large wood budget and transport dynamics on a large river using radio telemetry. Earth Surf Process Landf 39(4):487–498. https://doi.org/10.1002/esp.3463

79. Schmocker L, Weitbrecht V (2013) Driftwood: risk analysis and engineering measures. J Hydraul Eng 139(7):683–695. https://doi.org/10.1061/(Asce)Hy.1943-7900.0000728

80. SCHWEIZERFLUSS (2022a) 1_Limmat River - Description and Data. doi:https://schweizerfluss.ch/limmat/

81. SCHWEIZERFLUSS (2022b) 2_Thur River - Description and Data. doi:https://schweizerfluss.ch/thur/

82. SCHWEIZERFLUSS (2022c) 3_Grosse Melchaa River - Description and Data. doi:https://schweizerfluss.ch/grosse-melchaa/

83. Smart Solutions Technology (2020) Manufacturer of inertial measurement units for SmartWood. *Homepage:* . doi:www.agrobusiness-niederrhein.de

84. Spreitzer G, Gibson J, Tang M, Tunnicliffe J, Friedrich H (2019) SmartWood: laboratory experiments for assessing the effectiveness of smart sensors for monitoring large wood movement behaviour. CATENA. https://doi.org/10.1016/j.catena.2019.104145

85. Spreitzer G, Ravazzolo D, Tunnicliffe J, Friedrich H (2022) Measuring the impact: new insights into flood-borne large wood collisions with river

structures using an isolated sensor-unit. Nat Hazards. https://doi.org/10.1007/s11069-022-05354-3

86. Spreitzer G, Schalko I, Boes RM, Weitbrecht V (2022b) Quantification of large wood (LW) impact forces at field-scale using SmartWood. E-proceedings of the 39th IAHR World Congress Granada, Spain, June 2022.

87. Spreitzer G, Schalko I, Boes RM, Weitbrecht V (2022) SmartWood—Innovative Sensortechnik zur Messung und analyse von Schwemmholzprozessen in Fliessgewässern. Wasser Energie Luft 114(4):259–266

88. Spreitzer G, Tunnicliffe J, Friedrich H (2019b) Using smart sensors for measuring impact forces of large wood (LW). *E-proceedings of the 38th IAHR World Congress, Panama City, Panama, September 2019*. https://cpb-ap-se2.wpmucdn.com/blogs.auckland.ac.nz/dist/7/206/files/2020/11/c059.pdf

89. Spreitzer G, Tunnicliffe J, Friedrich H (2021) Effects of large wood (LW) blockage on bedload connectivity in the presence of a hydraulic structure. Ecol Eng 161:106156. https://doi.org/10.1016/j.ecoleng.2021.106156

90. Steeb N, Badoux A, Rickli C, Rickenmann D (2020) Detailbericht zum Forschungsprojekt WoodFlow - Verkleinerung von Schwemmholz. *Eidg. Forschungsanstalt für Wald, Schnee und Landschaft WSL*, 38. doi:https://woodflow.wsl.ch/fileadmin/user_upload/WSL/Microsite/Woodflow/Detailbericht_Schwemmholzverkleinerung.pdf

91. STK (2017) SCHWEMMGUT AN HOCHWASSERENTLASTUNGSANLAGEN (HWE) VON TALSPERREN in german. *Schweizerisches Talsperrenkomitee - Swiss Committee on Dams*. https://www.swissdams.ch/fr/publications/publications-csb/2017_Schwemmholz.pdf

92. Swanson FJ, Gregory SV, Iroumé A, Ruiz-Villanueva V, Wohl E (2021) Reflections on the history of research on large wood in rivers. Earth Surf Process Landf 46(1):55–66. https://doi.org/10.1002/esp.4814

93. Swanson FJ, Lienkaemper GW, Sedell JR (1976) History, Physical Effects, and management implications of large organic debris in western Oregon streams USDA forest service general technical report PNW-56, 21.

94. Tanaka N, Yagisawa J (2009) Effects of tree characteristics and substrate condition on critical breaking moment of trees due to heavy flooding. Landscape Ecol Eng 5(1):59–70. https://doi.org/10.1007/s11355-008-0060-5

95. TSCHUBBY (2022) Karte_Schweiz.png. *Wikimedia.org*. https://commons.wikimedia.org/wiki/File:Karte_Schweiz_Details.png

96. Turowski JM (2018) Alluvial cover controlling the width, slope and sinuosity of bedrock channels. Earth Surf Dyn 6(1):29–48. https://doi.org/10.5194/esurf-6-29-2018

97. Uchupi E, Jones G (1967) Woody debris on the mainland shelf off Ventura Southern California. Sedimentology 8:147–151

98. Warren DR, Kraft CE (2008) Dynamics of large wood in an eastern U.S. mountain stream. Forest Ecol Manag 256(4):808–814. https://doi.org/10.1016/j.foreco.2008.05.038

99. Wohl E, Iskin EP (2022) The transience of channel-spanning logjams in mountain streams. Water Resour Res. https://doi.org/10.1029/2021wr031556

100. Wohl E, Kramer N, Ruiz-Villanueva V, Scott DN, Comiti F, Gurnell AM, Piegay H, Lininger KB, Jaeger KL, Walters DM, Fausch KD (2019) The natural wood regime in rivers. Bioscience 69(4):259–273. https://doi.org/10.1093/biosci/biz013

101. Wyss A, Schalko I, Weitbrecht V (2021) Field study on wood accumulation at a bridge pier. Water. https://doi.org/10.3390/w13182475

102. X-Io Technologies (2021) Fusion simple_example.py Algorithm *Github.com*. https://github.com/xioTechnologies/Fusion/tree/main/Python

103. Yean S, Lee BS, Yeo CK, Vun CH, Oh HL (2018) Smartphone orientation estimation algorithm combining Kalman filter with gradient descent. IEEE J Biomed Health Inform 22(5):1421–1433. https://doi.org/10.1109/JBHI.2017.2780879

Publisher's Note